AD_____

Award Number: W81XWH-05-1-0480

TITLE: In Vivo Molecular Imaging of Mammary Tumorigenesis in Murine Model Systems

PRINCIPAL INVESTIGATOR: Margaret S. Saha, Ph.D.

CONTRACTING ORGANIZATION: The College of William and Mary
Williamsburg, VA 23185

REPORT DATE: August 2007

TYPE OF REPORT: Final

PREPARED FOR: U.S. Army Medical Research and Materiel Command
Fort Detrick, Maryland 21702-5012

REPORT DOCUMENTATION PAGE

Form Approved
OMB No. 0704-0188

1. REPORT DATE *(DD-MM-YYYY)*	**2. REPORT TYPE**	**3. DATES COVERED** *(From - To)*
01-08-2007	Final	1 AUG 2005 - 31 JUL 2007

4. TITLE AND SUBTITLE
In Vivo Molecular Imaging of Mammary Tumorigenesis in Murine Model Systems

5a. CONTRACT NUMBER

5b. GRANT NUMBER
W81XWH-05-1-0480

5c. PROGRAM ELEMENT NUMBER

6. AUTHOR(S)
Margaret S. Saha, Ph.D.

E-Mail: mssaha@wm.edu

5d. PROJECT NUMBER

5e. TASK NUMBER

5f. WORK UNIT NUMBER

7. PERFORMING ORGANIZATION NAME(S) AND ADDRESS(ES)

The College of William and Mary
Williamsburg, VA 23185

8. PERFORMING ORGANIZATION REPORT NUMBER

9. SPONSORING / MONITORING AGENCY NAME(S) AND ADDRESS(ES)
U.S. Army Medical Research and Materiel Command
Fort Detrick, Maryland 21702-5012

10. SPONSOR/MONITOR'S ACRONYM(S)

11. SPONSOR/MONITOR'S REPORT NUMBER(S)

12. DISTRIBUTION / AVAILABILITY STATEMENT
Approved for Public Release; Distribution Unlimited

13. SUPPLEMENTARY NOTES

14. ABSTRACT The development of accurate diagnostic tools and effective breast cancer treatments requires the ability to detect the presence of pre-cancerous, cancerous, and metastatic tissue and to identify the particular subtype or class of tumor. It is equally imperative to develop the capability of performing a "molecular diagnosis" non-invasively, employing *in vivo* imaging technologies in order to follow the tumor progression over time. This project entails an interdisciplinary approach which employs a gamma-ray-camera detector system to follow, during tumorigenesis, the uptake of NaI through the Na+/I- symporter, and the binding characteristics and localization of vascular endothelial growth factor, epidermal growth factor, and estradiol in mouse models of breast cancer. Using the MMTV model for mammary tumor development, we have found that I-125 labeled sodium iodide provides a valuable tag for imaging mammary tumors at several different stages of their development. Moreover, it is also able to provide an image of the heterogeneity among tumors and within a given tumor, making it potentially useful as a strategy for non-invasively imaging and classifying mammary tumors for purposes of prognosis.

15. SUBJECT TERMS
Mammary tumor; in vivo; imaging; breast cancer; mouse models

16. SECURITY CLASSIFICATION OF:			**17. LIMITATION OF ABSTRACT**	**18. NUMBER OF PAGES**	**19a. NAME OF RESPONSIBLE PERSON**
a. REPORT	**b. ABSTRACT**	**c. THIS PAGE**			USAMRMC
U	U	U	UU	35	**19b. TELEPHONE NUMBER** *(include area code)*

Table of Contents

INTRODUCTION

The development of accurate diagnostic tools and effective breast cancer treatments requires the ability to detect the presence of pre-cancerous, cancerous, and metastatic tissue and to identify the particular subtype or class of tumor. It is equally imperative to develop the capability of performing a "molecular diagnosis" non-invasively, employing *in vivo* imaging technologies in order to follow the tumor progression over time. This project entails an interdisciplinary approach which employs a gamma-ray-camera detector system to follow, during tumorigenesis, the uptake of NaI through the Na+/I- symporter (NIS) (Cho, 2002; Chung, 2003: Dadachova and Carrasco, 2004; Dadachova and Zuckier, 2003). This is a particularly useful marker for detecting and following the progression of mammary tumors. The project has also attempted to test other possible ligands as early markers for mammary tumors including vascular endothelial growth factor, epidermal growth factor, and estradiol. All of these molecules have been implicated as key players in the oncogenesis in breast cancer. Using a dual modality (gamma and x-ray) small animal detector system (H8500 Hamamatsu position sensitive photomultiplier tubes and a pixelated NaI(Tl) crystal array with a CuBe parallel-hole collimator), these radioactively tagged molecules are imaged over time in the same animal using a well characterized mouse model of breast cancer : mouse mammary tumor virus mice. In addition, these *in vivo* imaging data have been correlated with results obtained from gene expression studies using RT-PCR analysis and immunocytochemistry. Combining *in vivo* molecular imaging with gene expression technology has allowed us to establish potentially novel correlations between molecular markers and in vivo data sets. Our ability to detect iodine metabolism within tumors as well as size and pattern may serve as an important diagnostic tool.

BODY OF REPORT

As specified in our Statement of Work document, the research has focused on (1) making our detector system functional for the imaging of mammary tumors; (2) using the MMTV breast cancer tumor model to conduct an extensive series of imaging with I-125 labeled sodium iodide to image NIS expression as well attempting additional ligands includingTGF-alpha, estradiol and VEGF; (3) conducting an extensive series of analyses using the imaging data to draw conclusions regarding the use of these compounds as imaging agents for breast cancer; and performing the molecular work linking the imaging data to the molecular events. A significant amount of effort has been devoted to the analysis of our data. We summarize our research progress by describing the key issues which our work successfully addressed throughout the course of the grant.

Detector and Technology Development

We have developed a compact gamma camera, sized particularly for imaging a mouse. The active area of the detector is approximately 46 mm x 96 mm. Two flat-panel Hamamatsu H8500 position-sensitive photomultiplier tubes (PSPMTs) are coupled to a pixellated NaI(Tl) scintillator which views the animal through a copper-beryllium (CuBe) parallel-hole collimator specially designed for ^{125}I (~35 keV, 60-day half life). For this mammary tumor MMTV study, a collimator was implemented providing high efficiency and reasonable resolution (slightly above 2 mm) for planar imaging. Furthermore, the proof-of-concept studies of mouse thyroid and mammary tumor have demonstrated the feasibility of parallel-hole single photon emission computed tomography (SPECT) using the compact detector. To further improve the reconstructed resolution of SPECT, we have expanded our imaging system by incorporating multipinhole helical SPECT using a 110 mm circular detector and a copper collimator with multiple 1-mm diameter pinholes. An in vivo study has demonstrated clear delineation of the two lobes (usually separated by 1.8-2.5 mm) of a mouse thyroid using two-pinhole helical SPECT and a dose as small as 200 µCi. Combining planar scintigraphy and tomography, this imaging system has the potential for a variety of preclinical applications. Now we are developing a

novel square detector with double active area of the “mouse-sized” detector, in which 3 mm thick single slate of $LaBr_3$ scintillator and four Hamamatsu H9500 PSPMTs are incorporated. $LaBr_3$ is a newly available scintillator with better energy resolution and sensitivity while H9500 modules provide higher intrinsic resolution than the H8500 modules used in the “mouse-sized” detector. This novel detector will not only allow us to image two mice simultaneously for immediate comparison of their response to radiotracers, but also enable large field-of-view multipinhole helical SPECT or slit-slant SPECT.

Work conducted using I-125 labeled ligands to image mammary tumors in MMTV tumor animals:

Imaging with VEGF, TGF-alpha, and estradiol

I n addition to using I-125 NaI for imaging mammary tumors (described in detail below), three additional I-125 labeled compounds were used: vascular endothelial growth factor, transforming growth factor alpha, and estradiol. Each of these were used on three different mice with tumors at various stages, however none of these ligands were able to effectively and reliably detect mammary tumors to any significant degree. Therefore our work focused on the promising new information produced by imaging sodium iodide and its transporter.

Work conducted using I-125 NaI to image mammary tumors in MMTV tumor animals:

Validating Gamma Imaging with Molecular Assays

^{125}I saturation relies on the NIS, a plasma membrane protein, for proper metabolism of iodide in receptive tissues. Immunohistochemistry was the avenue we took to localize this important protein with the use of antibodies that would bind to the protein itself. To visualize where the antibodies and protein concentrated in tumor tissue a secondary antibody was added to bind to the previously administered antibody. This secondary antibody fluoresces green (Alexa 488). Therefore in the images below the presence of the green signal indicates the presence of the NIS protein.

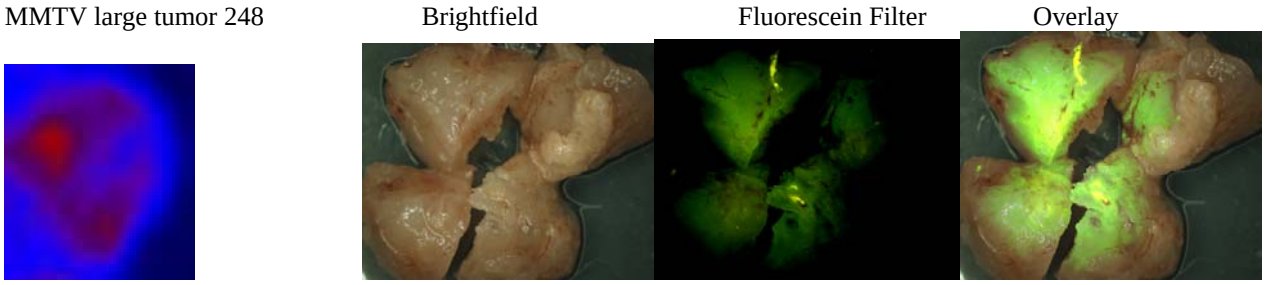

The four figures above correspond to a large MMTV tumor that underwent assay with immunohistochemistry. The leftmost image is the image created by the gamma camera. The tumor was divided into four quadrants for better (see brightfield) access to the antibodies. The green signal in the fluorescein filtered image represents to locality of the NIS protein in the tumor quadrants, while the overlay image provides both tumor morphology and NIS locality. From the overlay image the upper left quadrant had the greatest staining for the NIS which corresponds to the hottest upper left quadrant of the gamma image on the far left. The other three quadrants have lower amounts of staining for the NIS with upper right quadrant displaying the least, which correlates well with the upper right region of the tumor from the gamma camera on the photo far left. Also of note the lower right quadrant has a bright fluorescent stain that appears almost yellow. If you look at the lower right quadrant area of the left-most image you notice a hot linear uptake of ^{125}I in this quadrant.

MMTV small tumor 248

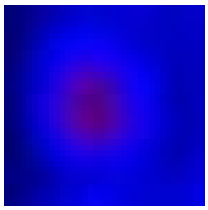

Brightfield

Fluorescein Filter

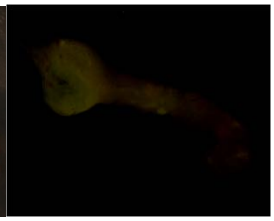

Overlay

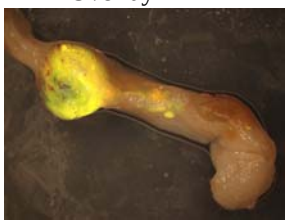

Above is the right inguinal mammary of the tumo- bearing mouse discussed previously. This gland was excised due to the hot spot seen in the left-most image. Before excision the assumption was that this was a normal gland that was metabolizing a high amount of ^{125}I. When dissected a noticeable small tumor (3mm diameter) was beginning to form to one end of the mammary gland (see brightfield). After immunohistochemical staining to localize the NIS there was a clear variation in the presence of the NIS in the small tumor area compared to the normal mammary tissue beside it (see overlay). Therefore, the gamma camera was able to detect a small tumor in the mouse where the circular hot spot of the left-most image corresponds to the circular tumor on the mammary gland of the overlay image. This was detected using imaging (a non-palpable tumor) and confirmed using a molecular assay.

Analysis of Imaging Data:

1. How many MMTV cases? How many are re-imaged? How many tumors are comparable?

A total of 42 “good” MMTV imaging cases (of 35 mice with 49 tumors in total) were analyzed including one mouse imaged three times and 5 mice imaged twice. Here, "good" means a full-hour imaging with no KI-blocking. The tumors are excluded if they are so close to the thyroid that they could cause significant errors. Finally we have a total of 62 tumor ROIs (Regions of Interest) (including imaged repeatedly) for comparison.

Distribution of the 35 mice bearing multiple tumors:

1-tumor mice	2-tumor mice	3-tumor mice
19	15	1

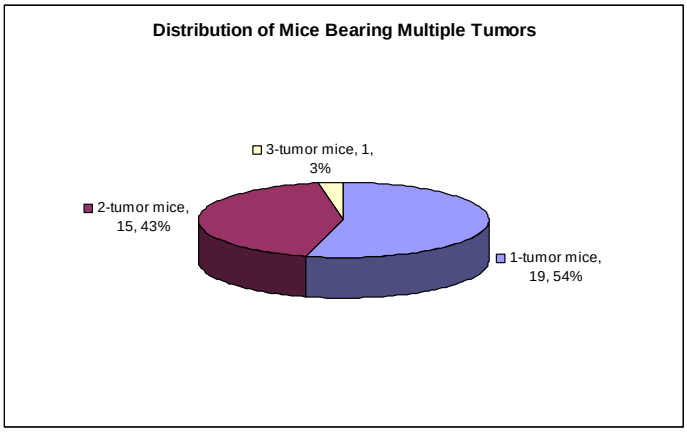

Location Distribution of the tumors of the 35 mice:

Left thoracic	Left inguinal	Right inguinal	Right thoracic
18	3	10	18

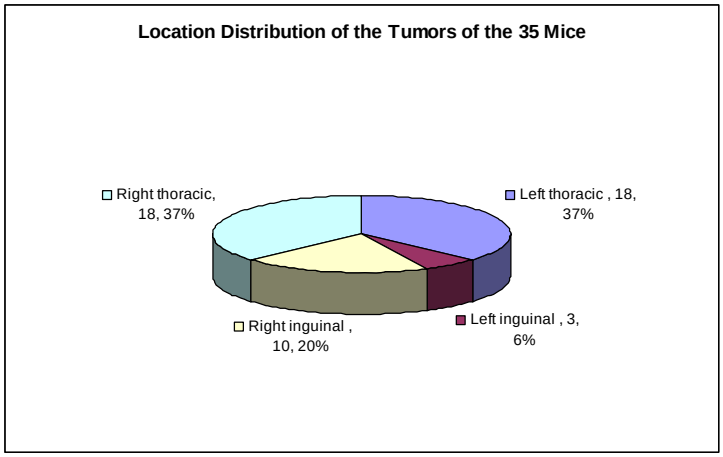

Thoracic tumors take a significant portion (about 74%) of the total 49 tumors. Only about 26% of the tumors locate in inguinal regions, suggesting that thoracic tumors are more possible to be developed in MMTV mice.

2. How is Background or "Threshold" Determined?

Using the method we developed, we can get the boundary of a tumor by subtracting a select threshold from the raw ROI of the tumor. The single-pixel-size threshold is the mean of 2x2 ROIs from all the time periods. The normalized thresholds used for the analysis was mainly distributed in the range (0.0004, 0.0007). This is also the I-125 level of heart at 60 min after injection when the distribution of I-125 in the blood flow is near stable. Therefore, the threshold deduction from a tumor ROI may avoid the misleading information due to blood flow and justify our usage to get the tumor size.

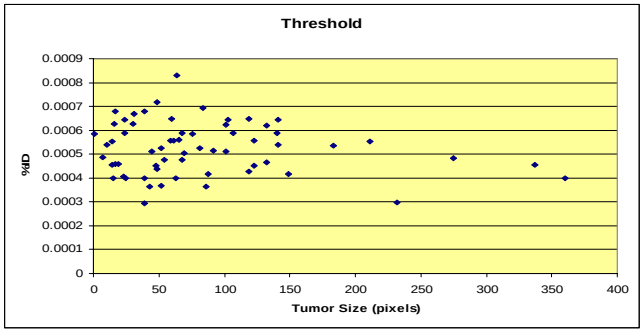
Threshold
0.0009
0.0008
0.0007
0.0006
0.0005
0.0004
0.0003
0.0002
0.0001
0
%ID
0
50
100
150
200
250
300
350
400
Tumor Size (pixels)

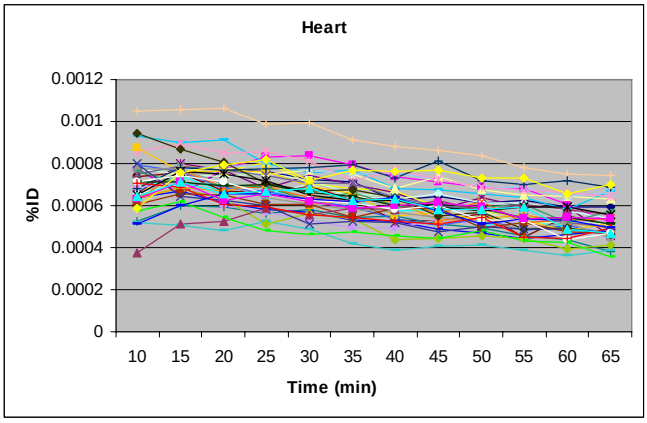
Heart
0.0012
0.001
0.0008
0.0006
0.0004
0.0002
0
%ID
10
15
20
25
30
35
40
45
50
55
60
65
Time (min)

3. Curve of Tumor Size with Time

We determined the tumor size by counting the number of non-zero pixels in the tumor ROI after threshold deduction. Since the tumor size at different time period may be different and the threshold representing the blood flow is taken out, a curve of tumor size vs. time may reveal when isotope I-125 is distributed to all over the tumor owing to NIS expression. All the tumor size curves were plotted in the following figure.

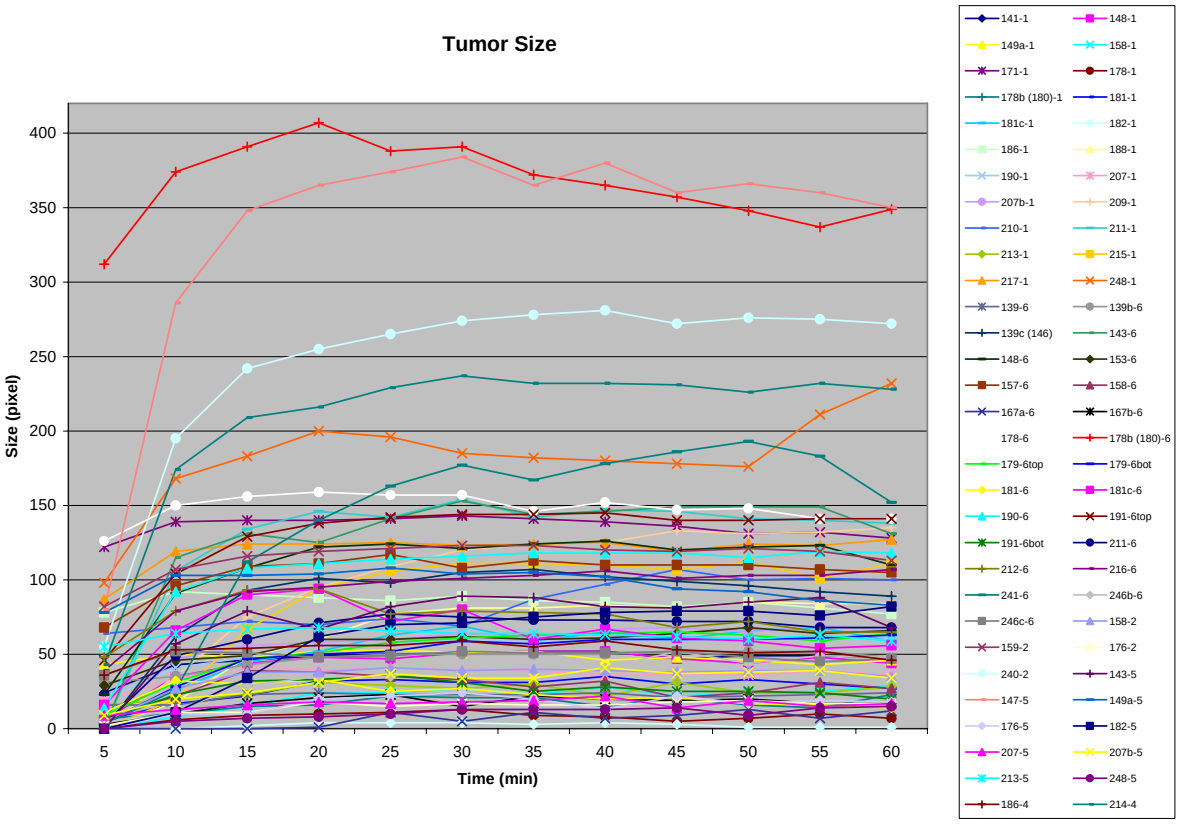

The figure indicates that, for the majority of the tumors, I-125 through NIS expression reaches about 90% of their tumor size at around 15-20 minute after injection disregarding the tumor size. I-125 reaches everywhere (maximum calculated tumor size) for 52 (~ 85%) tumors in 20-40 minutes after the injection, However, the calculated tumor size of 45 (73%) tumors starts to decrease after that, which may suggest decreased NIS expression in the tumor.

4. Patterns of I-125 Uptake in a Tumor

There are five patterns of I-125 uptake in the tumors:

Edge-to-Center Pattern: initially hot at the edge but finally hot within the central tumor

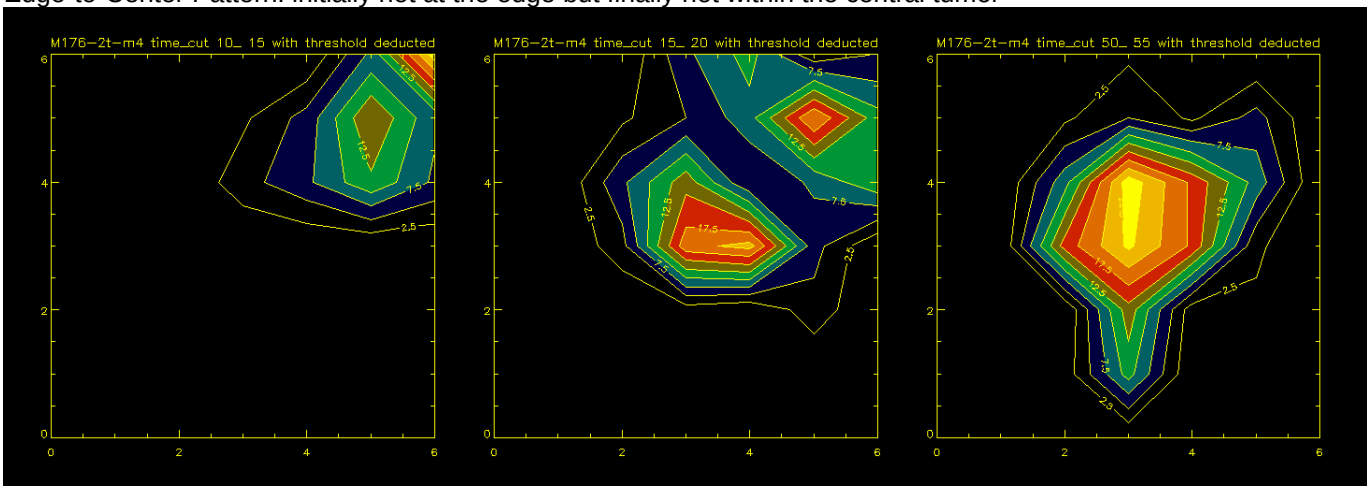

Center-to-Edge Pattern: always hot in one region and expand to nearby or farther tissues with time

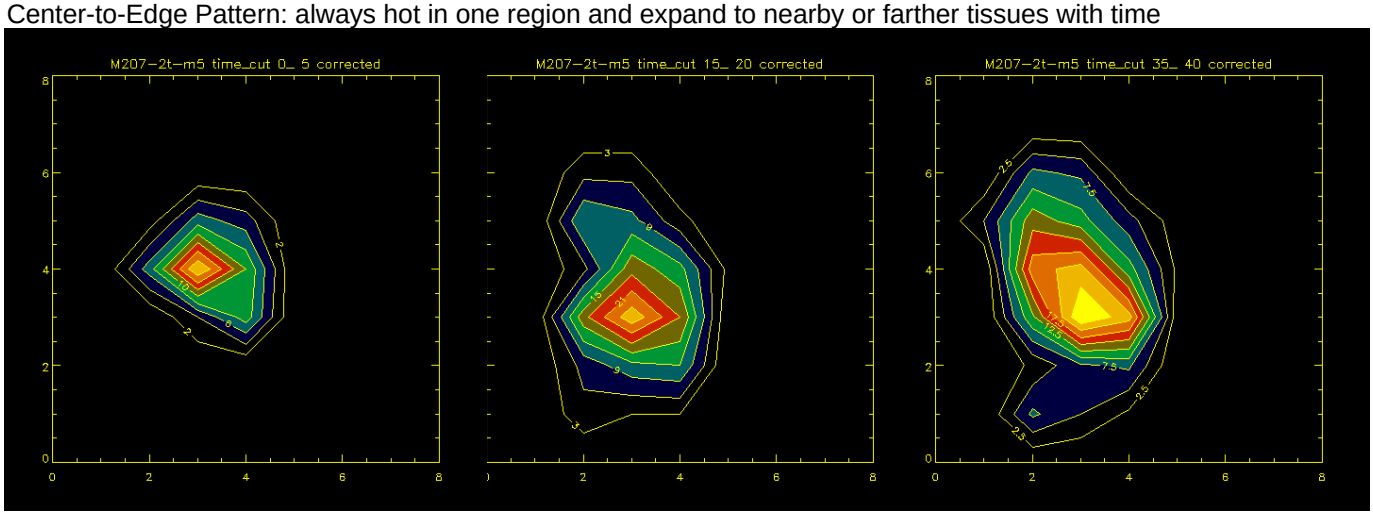

Multi-Spot Pattern: initially hot at one or more spots, then at other spots and/or their nearby tissues

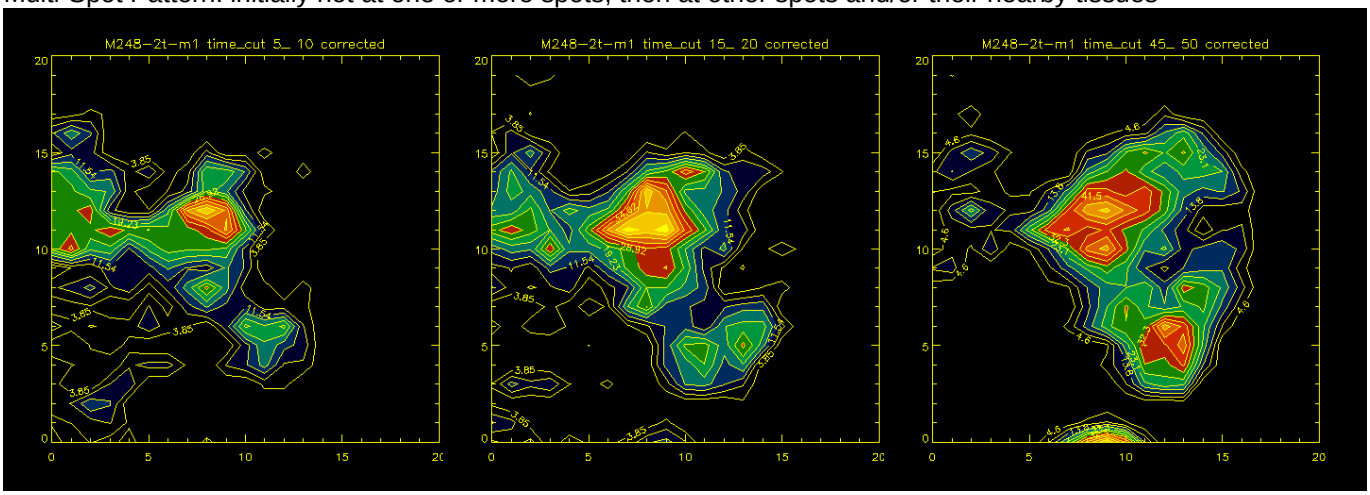

The pattern combining Edge-to-Center and Multi-Spot Patterns:

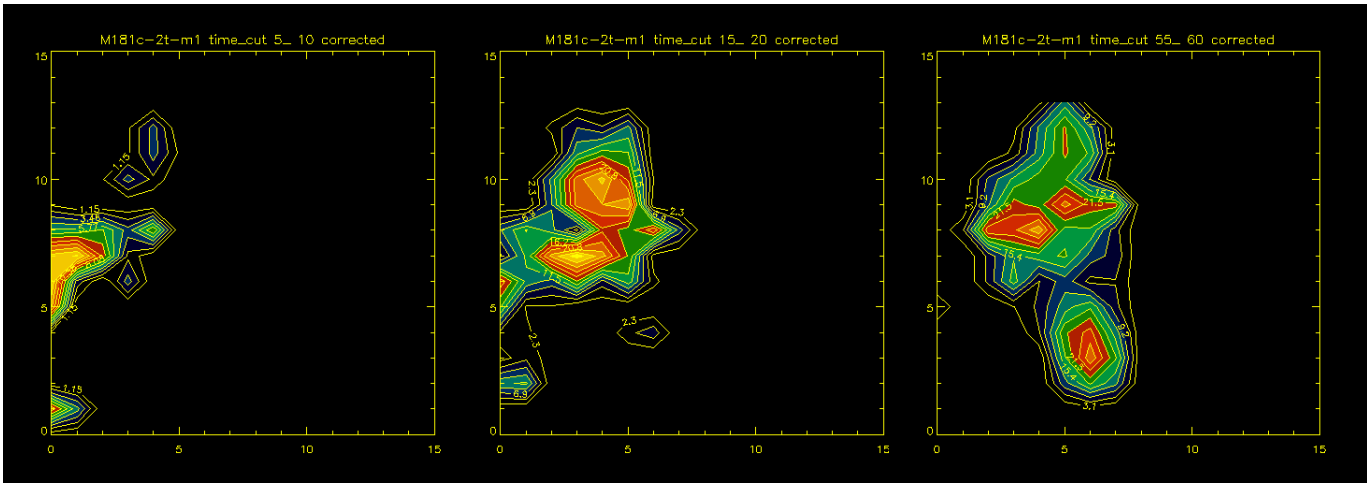

Ring pattern (a special pattern of multi-spot pattern) : a ring shape of I-125 uptake

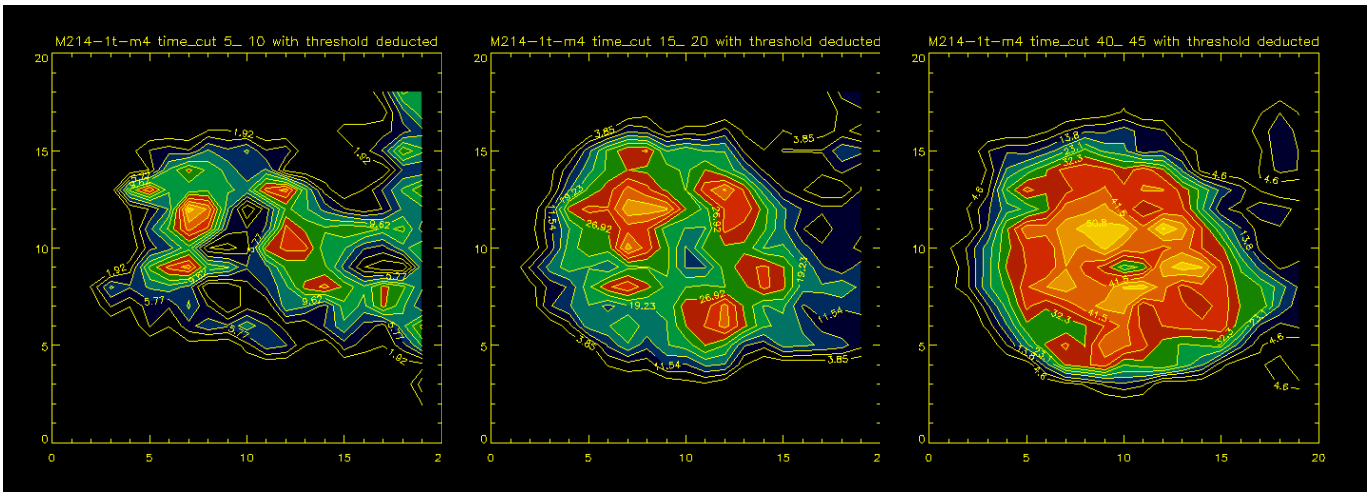

5. Correlation between tumor patterns and tumor size

A. Correlation between tumor patterns and near-stable (50_55 min) tumor sizes:

After getting the tumor size curve, we choose the tumor area (in pixel) at time-cut 50_55 as the actual size of the tumor.

Tumor (pixel)	edge-to-center	center-to-edge	multi-spot pattern	edge-to-center/multi-spot	ring
1-50	7	13	3	1	
51-100	3	5	7	1	1
101-150			13		
>150			1	2	3

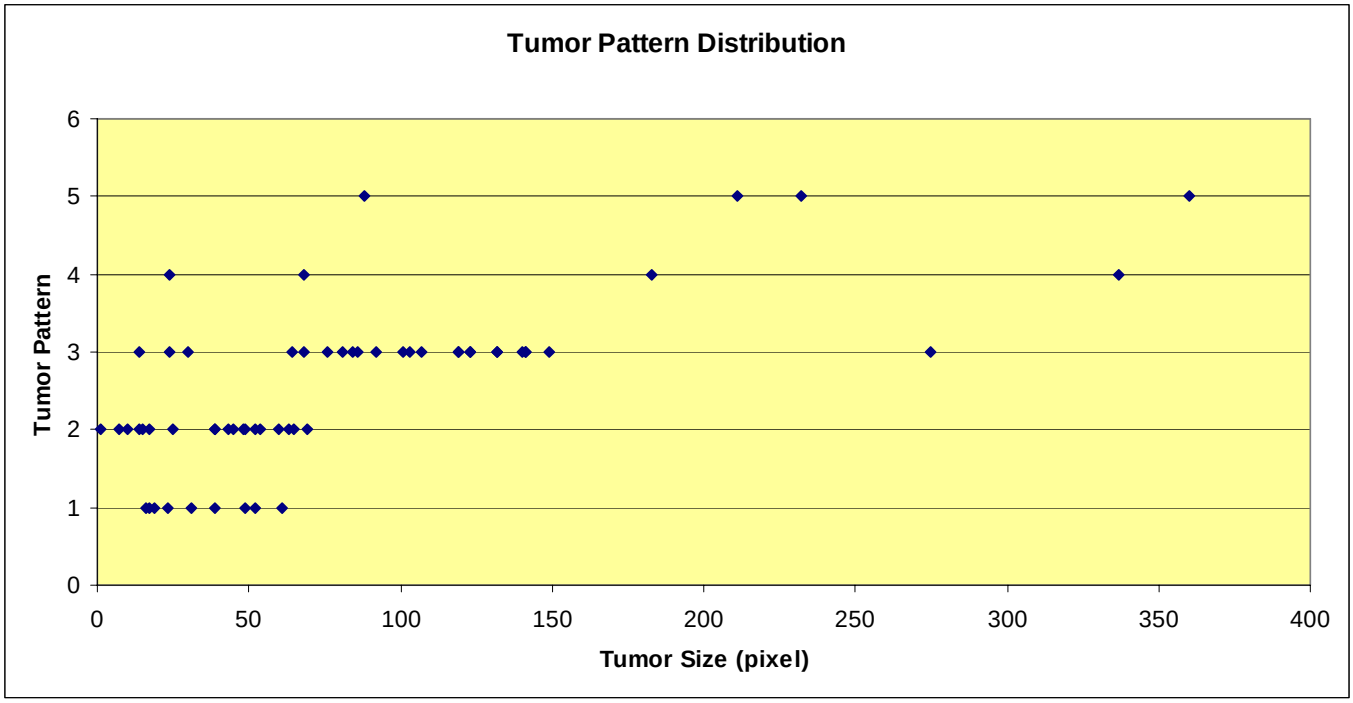

pattern 1:	Edge-to-Center
pattern 2:	Center-to-Edge
pattern 3:	Multi-spot
pattern 4:	Edge-to-Center/Multi-spot
pattern 5:	Ring (a special case of multi-spot pattern)

As shown in the table and figure, center-to-edge and edge-to-center patterns dominate the tumors with size below 65 pixels, in which 18 tumors (56%) are center-to-edge pattern and 10 (31%) are edge-to-center pattern. However, all the tumors with size above 65 pixels only have the multi-spot pattern or patterns related to it. Given that a small- or moderate-size tumor is usually a solid tumor, this correlation may suggest that solid tumors probably presents center-to-edge and edge-to-center patterns of I-125 uptake while necrotic tumors such as the tumors with size above 65 pixels show multi-spot pattern or those patterns associated with it.

B. Correlation between tumor patterns and dynamic curves of tumor sizes:

Each of the following dynamic curves of tumor size is averaged from three tumors (n = 3) with the same pattern and dynamic trend in the same range of tumor size. We treat ring and edge-to-center/multi-spot patterns as multi-spot patterns because they are either a special multi-spot pattern or a pattern related to it. The other reason for such treatment is because we have only 8 samples distributed in a large range of tumor size. They may be not sufficient for statistics.

(i) tumor size <= 50 pixels:

Two dynamic trends for edge-to-center pattern:

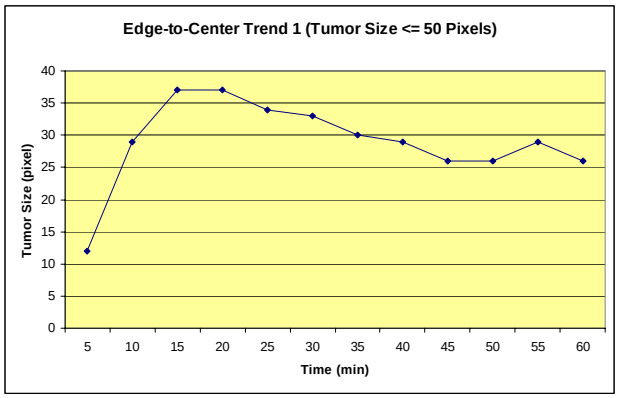

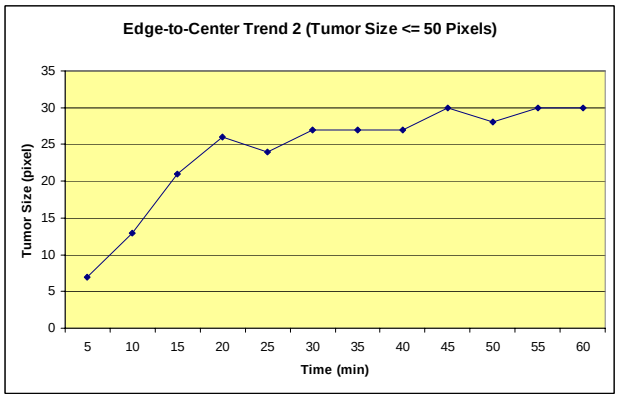

Two dynamic trends for center-to-edge pattern:

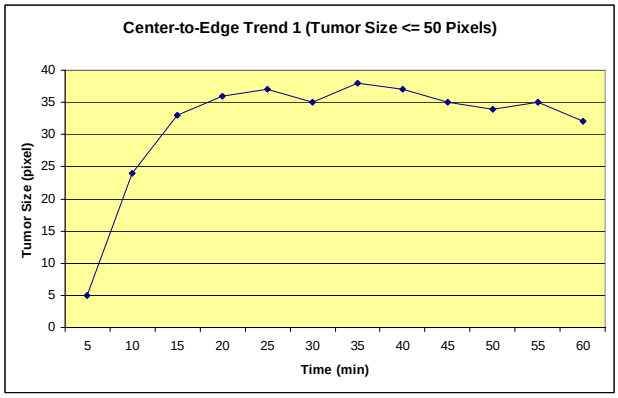

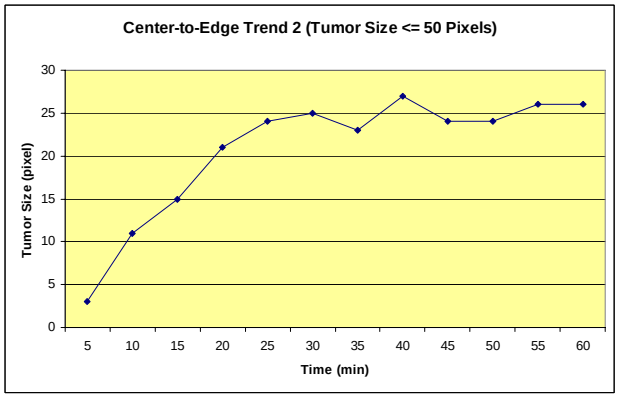

One dynamic trend for multi-spot pattern:

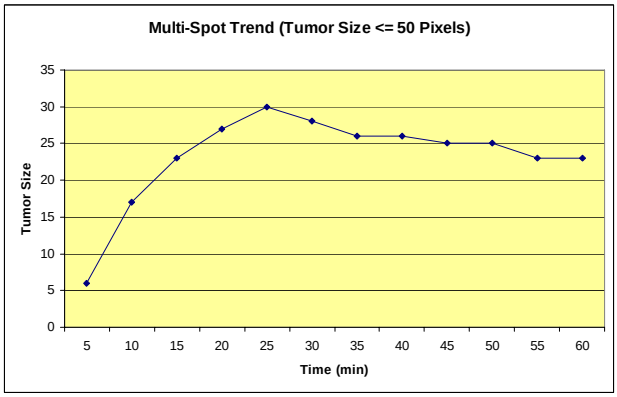

(ii) 50 < tumor size <= 100 pixels:

One dynamic trend for edge-to-center pattern:

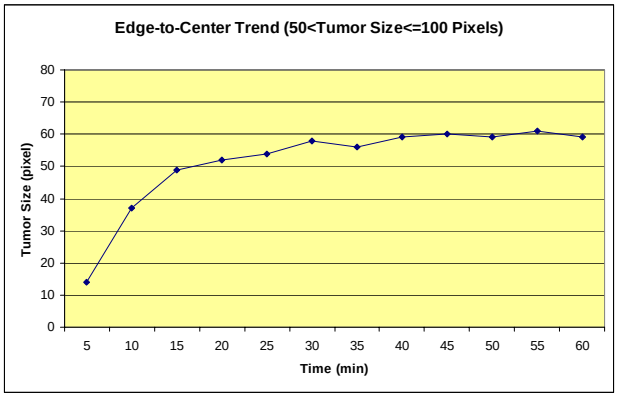

Two dynamic trends for center-to-edge pattern:

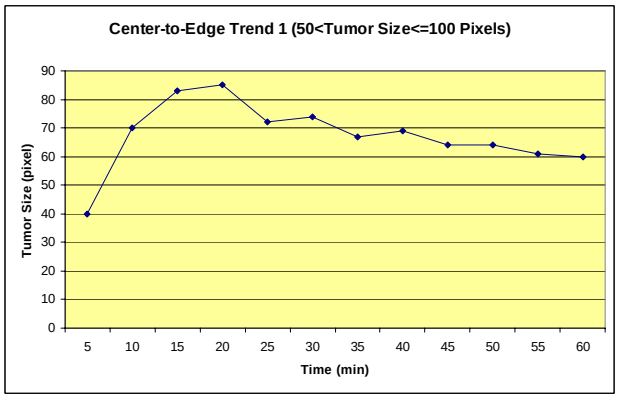

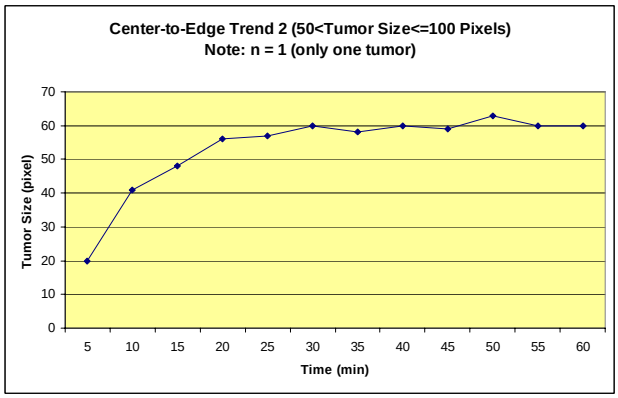

Two dynamic trends for multi-spot pattern:

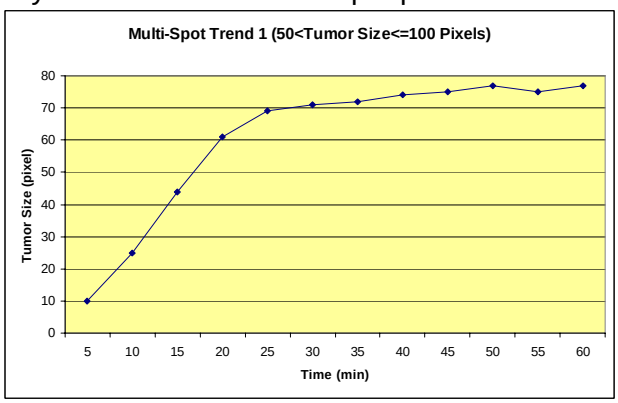

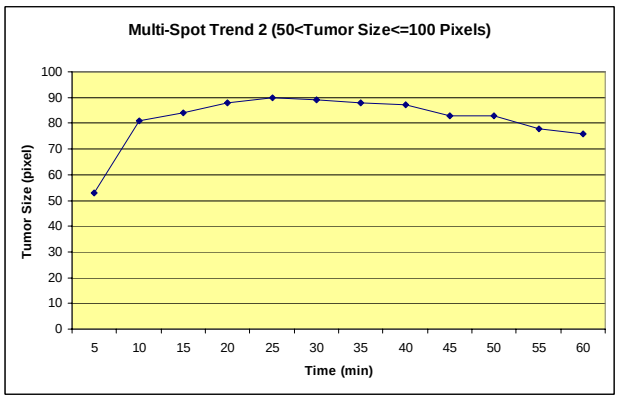

(iii) 100 < tumor size <= 150 pixels:

Two dynamic trends for multi-spot pattern:

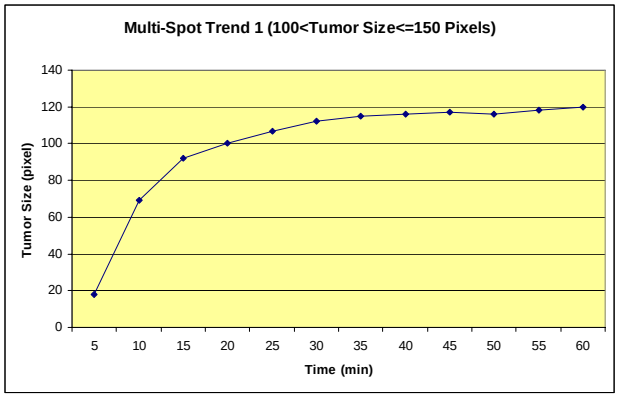

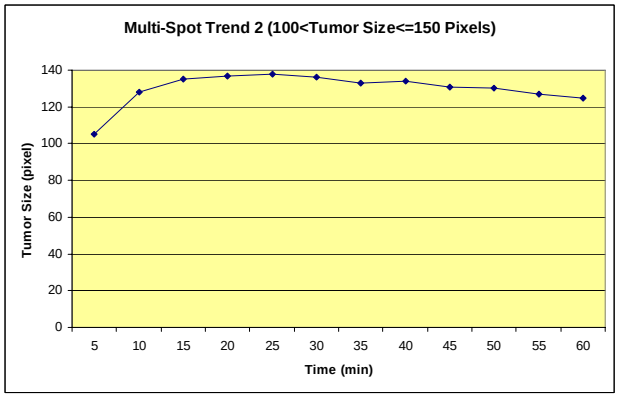

(iv) tumor size > 150 pixels:

One dynamic trend for multi-spot pattern:

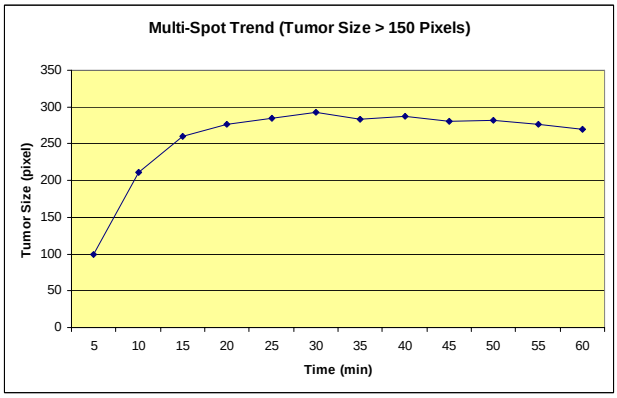

6. Correlation among Near-Stable I-125 Uptake, Tumor Pattern and Size

Again, we choose the tumor area (in pixel) at time-cut 50_55 as the actual size of the tumor. The total counts of that area at the same time cut with threshold deducted was considered as the near-stable uptake of I-125 in the tumor. Since the total injection dose is a variable for different mice, the total counts was normalized to the whole body as a percentage of injection dose (%ID). The correlation among the tumor patterns, size and the normalized dose of I-125 in the whole tumor was shown in the first figure, which reveals:

1. The total uptake of I-125 in the tumors with area < 50 pixels is pretty much similar (< 0.02). One may note the majority of tumors having edge-to-center or center-to-edge pattern dwell in this range of tumor size.
2. The tumors with area between 50 and 150 pixels show great variation of I-125 level. One may note two trends: some tumors show linear relationship between the I-125 level and tumor size while others present nonlinear (like exponential) relationship. The I-125 level of tumors with area around 130 pixels is comparable to the big/advanced tumors (area > 150 pixels). The two trends may suggest that tumors in study have three stages: tumors still in development with little necroses, tumors in development with moderate amount of necrotic tissue, and tumors with major necrotic tissue. On the other hand, the fact that multi-spot pattern dominate tumors in this range confirms that they are mainly necrotic tumors.

3. I-125 uptake in the tumors at advanced stage (>150 pixels) reaches a constant level (0.08). Given the large size, this may suggest that the advanced tumors are mainly necroses and that I-125 uptake in them probably comes from blood flow instead of NIS expression. The patterns of all the tumors in this range are multi-spot or patterns related to it, confirming that they are all necrotic tumors.

Presented in the second figure is the relationship among the tumor patterns, size and the normalized mean dose/pixel in the tumor. In addition to the above conclusions, this figure indicates that tumors with the most NIS expression are in the size of 50-100 pixels.

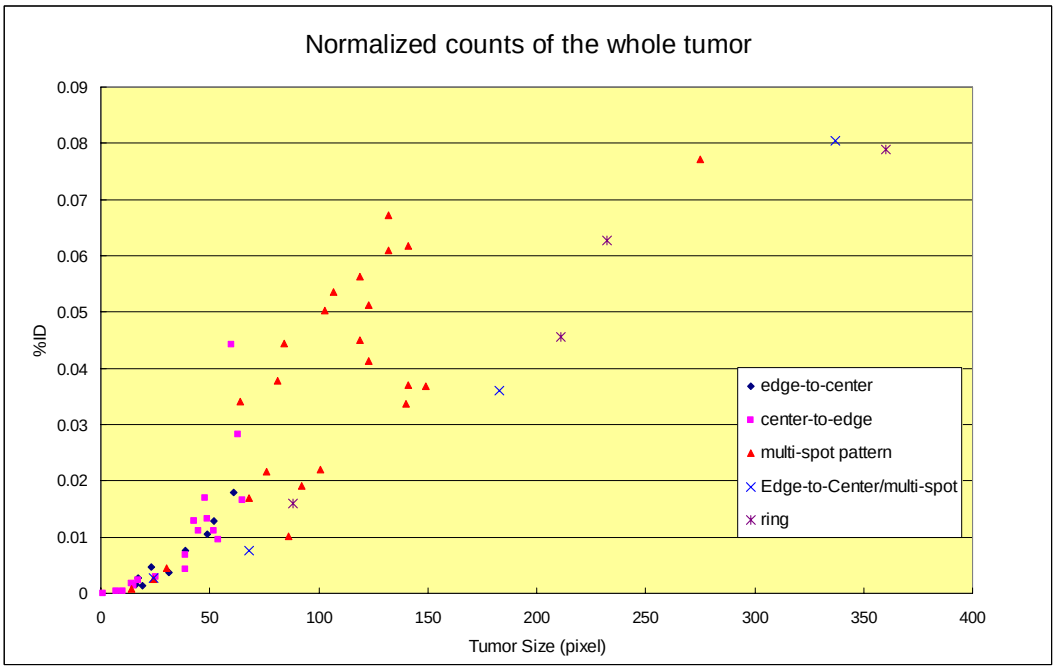

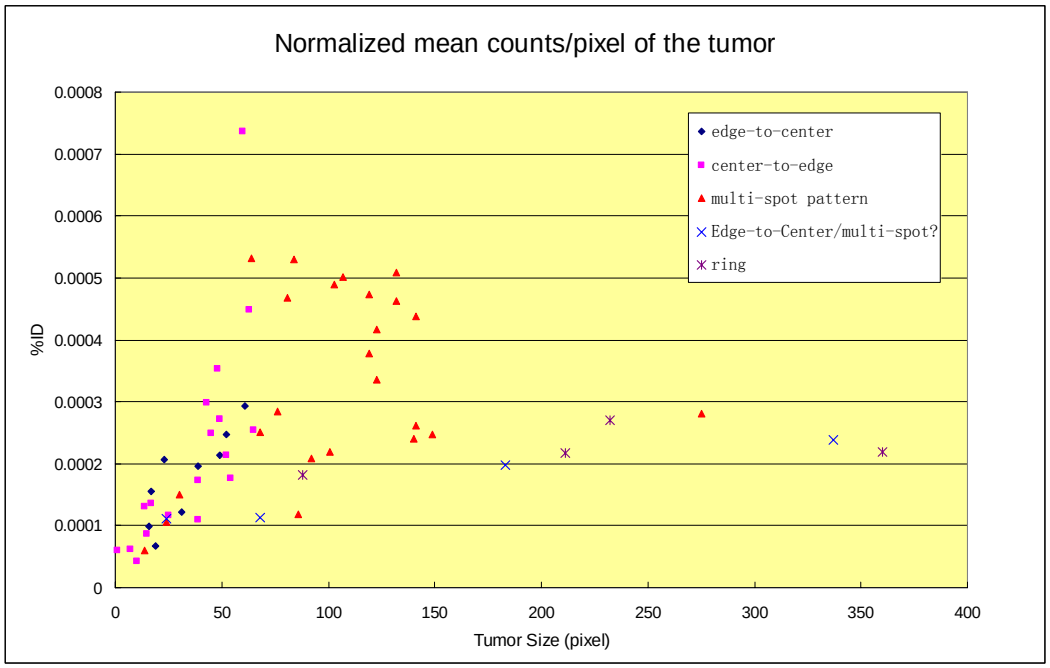

7. Correlation among Dynamic I-125 Uptake Trend, Tumor Pattern and Size

Similar to the correlations between tumor patterns and dynamic tumor size, the correlations among tumor patterns, dynamic I-125 uptake and tumor size are concluded here. Again, each of the following dynamic curves is averaged from three tumors (n = 3) with the same pattern and dynamic trend in the same range of tumor size.

(i) tumor size <= 50 pixels:

Two dynamic trends for edge-to-center pattern:

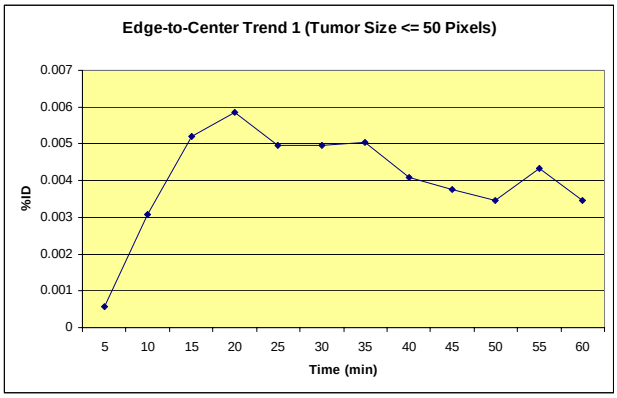

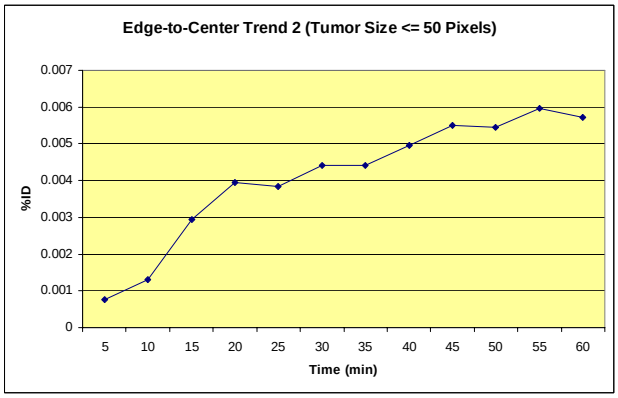

Two dynamic trends for center-to-edge pattern:

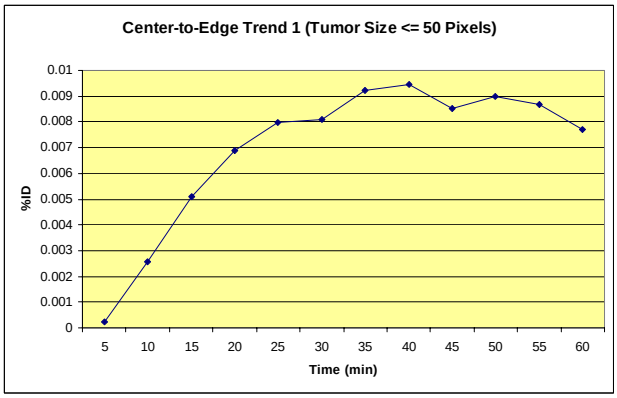

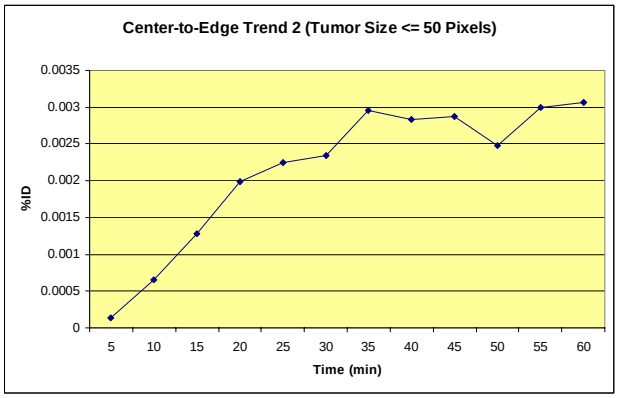

One dynamic trend for multi-spot pattern:

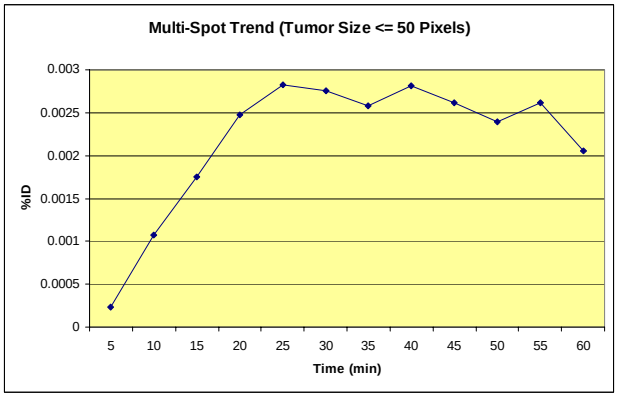

(ii) 50 < tumor size <= 100 pixels:

One dynamic trend for edge-to-center pattern:

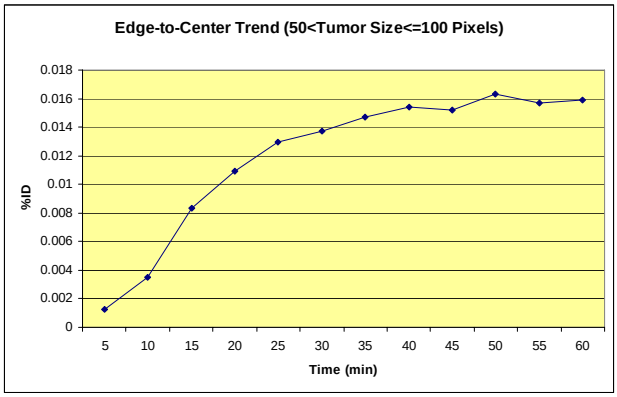

Two dynamic trends for center-to-edge pattern:

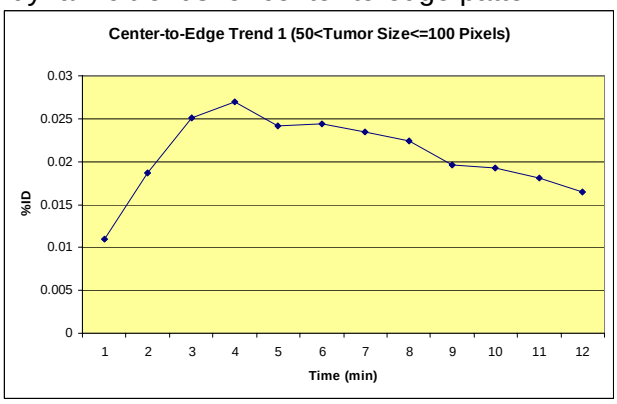

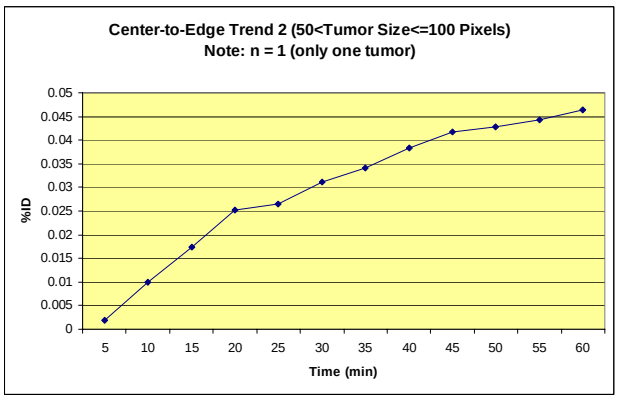

Two dynamic trends for multi-spot pattern:

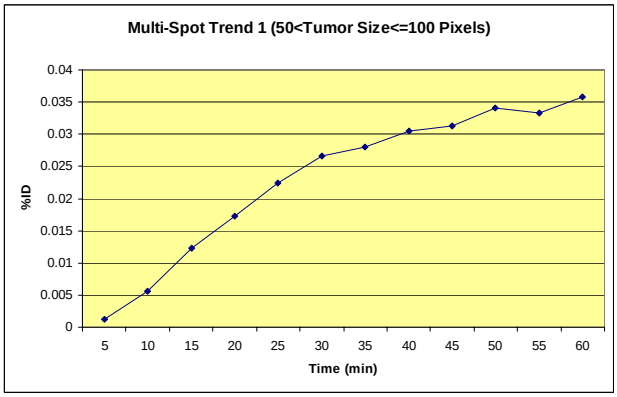

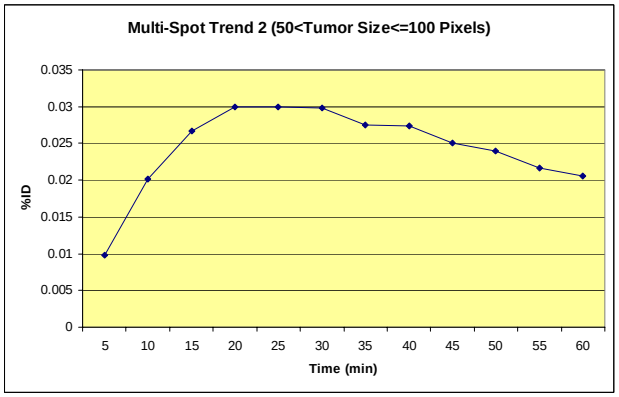

(iii) 100 < tumor size <= 150 pixels:

Two dynamic trends for multi-spot pattern:

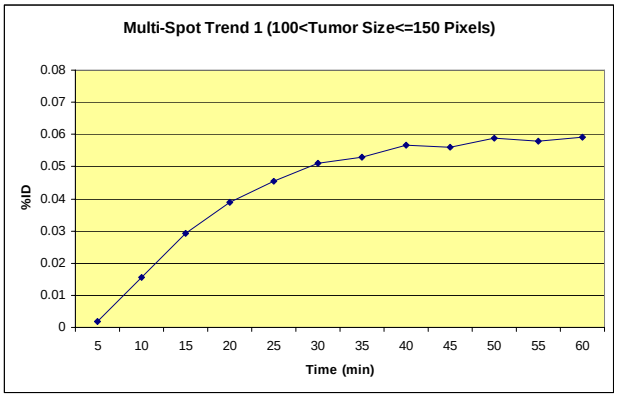

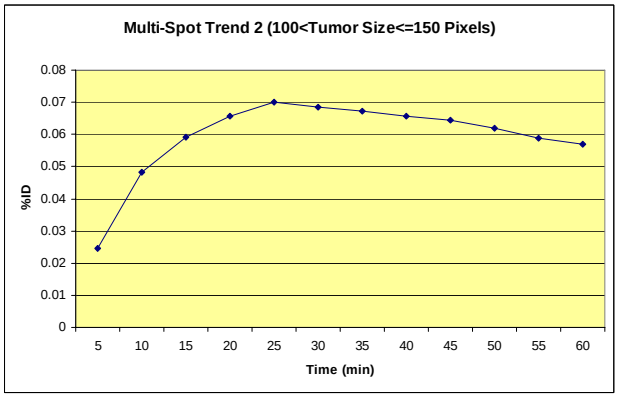

(iv) tumor size > 150 pixels:

One dynamic trend for multi-spot pattern:

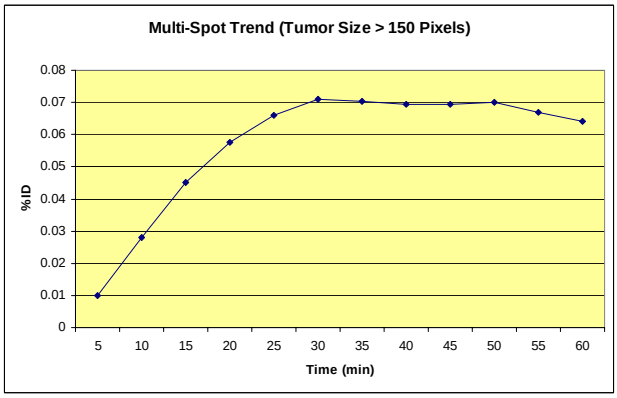

8. Difference Plots

Three sets of difference plots (plots analyzing difference between one time point and another) were analyzed: 0-5 min vs. 5-10 min, 25-30 min vs. 30-35 min, and 50-55 min vs. 55-60 min. Here, every timecut is raw ROI data without threshold deduction. The difference between each set of timecuts was calculated by deducting the early timecut from the late timecut. The positive and negative values were then put in a positive plot (counts increase along time) and a negative plot (counts decrease along time) respectively. After comparing a timecut near the end of one-hour imaging such as 50-55 min with the positive difference plot between 0-5 min and 5-10 min timecuts, we may note they are correlated in the pattern.

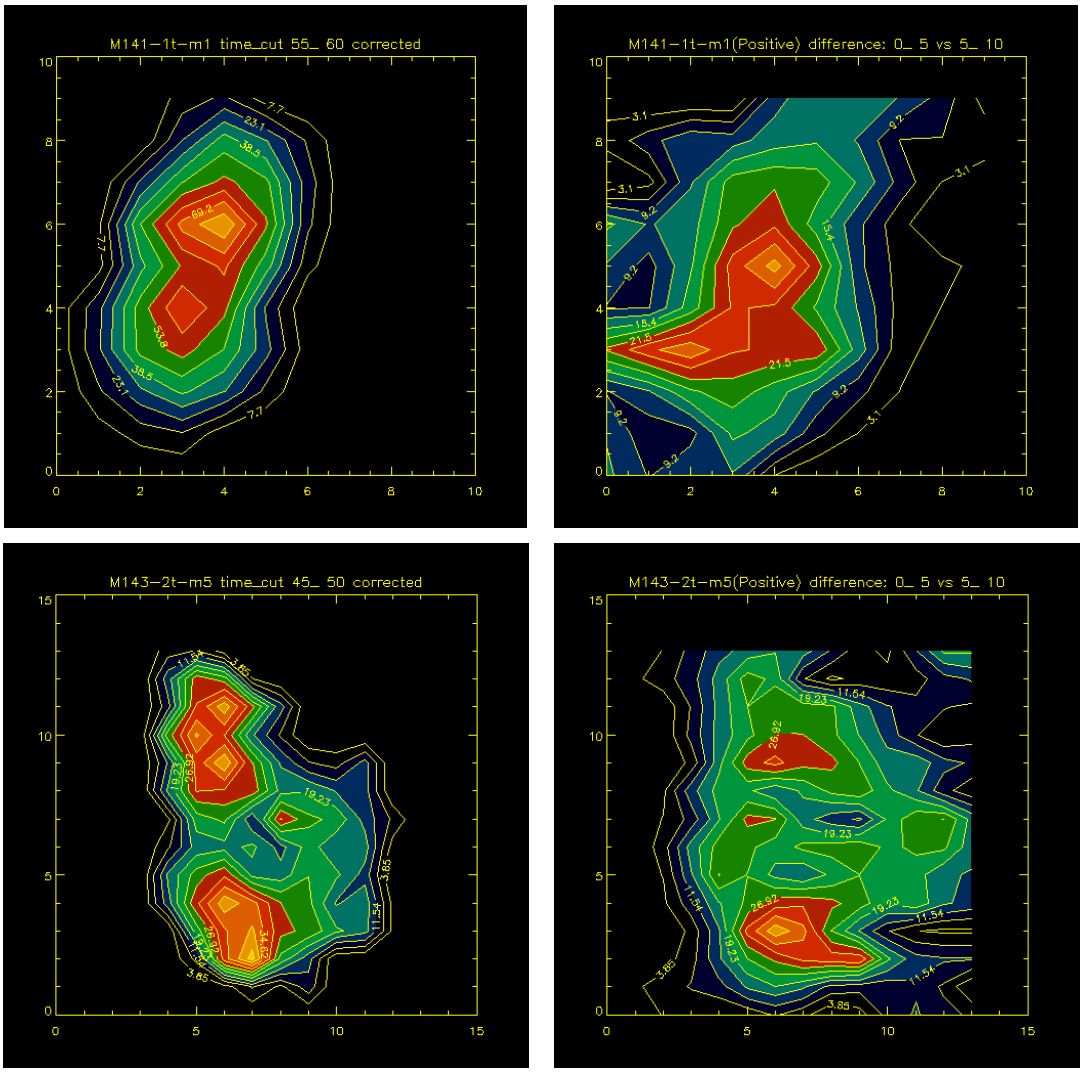

The location and intensity of NIS expression in a tumor shown in a gamma-ray image correlate with the image from immunohistochemistry. A timecut such as 50-55 or 55-60 min can represent the gamma-ray image Eric Blue used in his work. The hotter the tumor region in the timecut, the stronger the NIS expression in that region. His work also confirmed that the NIS expression mainly came from the active tumor tissues. Therefore, the correlation between the timecut near the end of the imaging and the positive difference plot at the beginning of the imaging may reveal that NIS expression of the active tumor tissues is the major contributor to I-125 uptake in the tumor at the beginning. The advantage of the positive difference plot is that it may reveal the actual loci of active tumor tissues in the tumor. This information may be not clear in a late-period timecut. For example in the following figures of mouse 148, we may tell from the 50_55 timecut that NIS expression is mainly in the central region. However, the difference plot in the right gives us more detail that major NIS expression happens at three loci in the tumor.

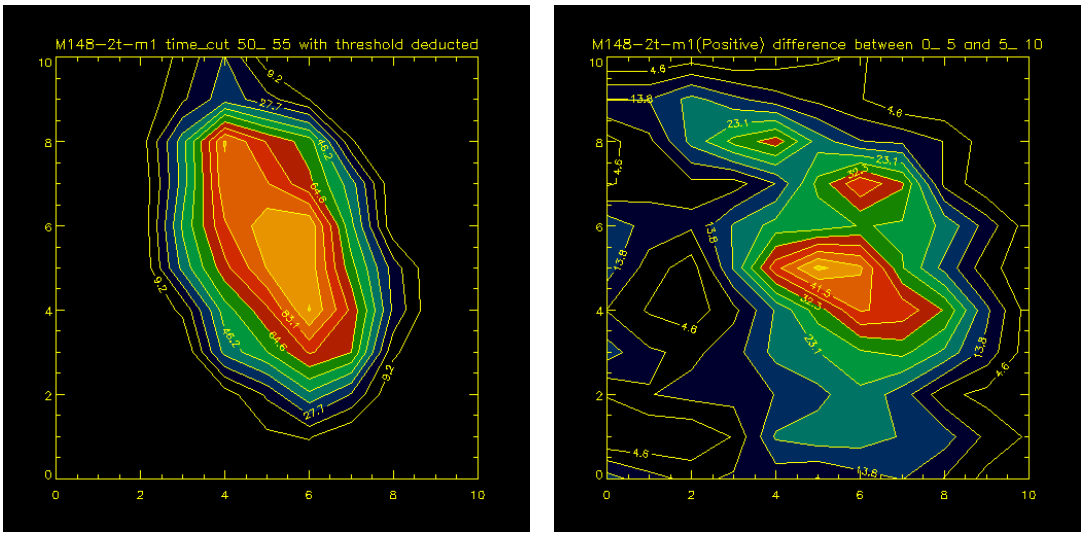

As the time-course I-125 uptake curves indicate, the counts of the tumor ROIs reach platform or maximum for 84% tumors (52) at around 30 min after the injection. In this case, the positive difference plots of the last two sets of timecuts reveal that the major contributor of I-125 uptake in the tumor is not from those active tumor tissues but from the tissues adjacent to them or tissues farther from them in time order (see the following positive difference plots of mouse 248).

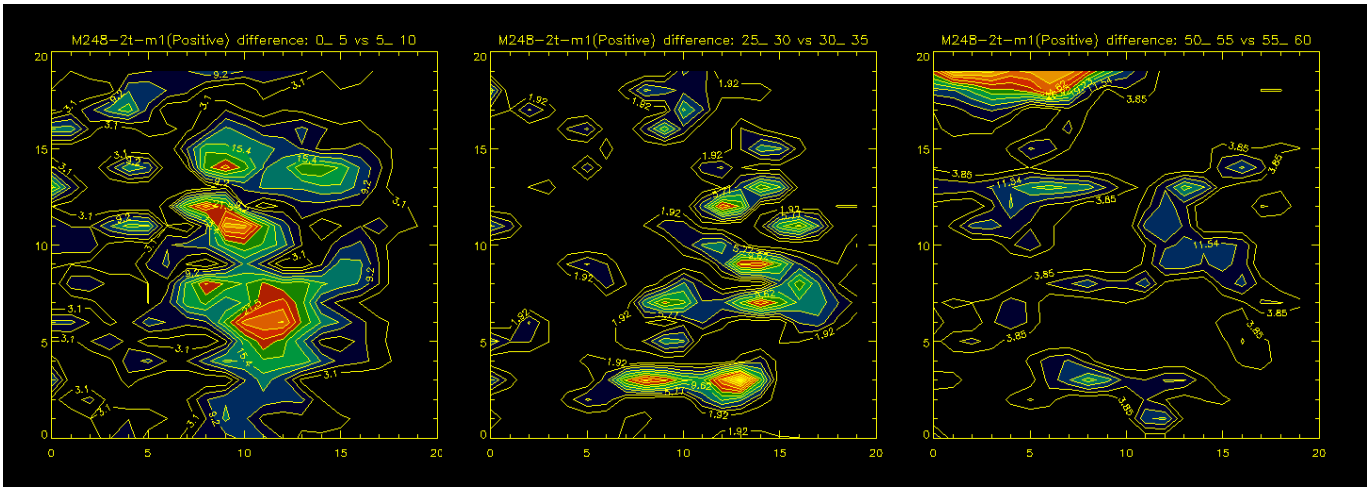

For the tumors presenting continuous uptake of I-125, the positive difference plots indicate that some active tumor tissues were expressing NIS across the imaging time.

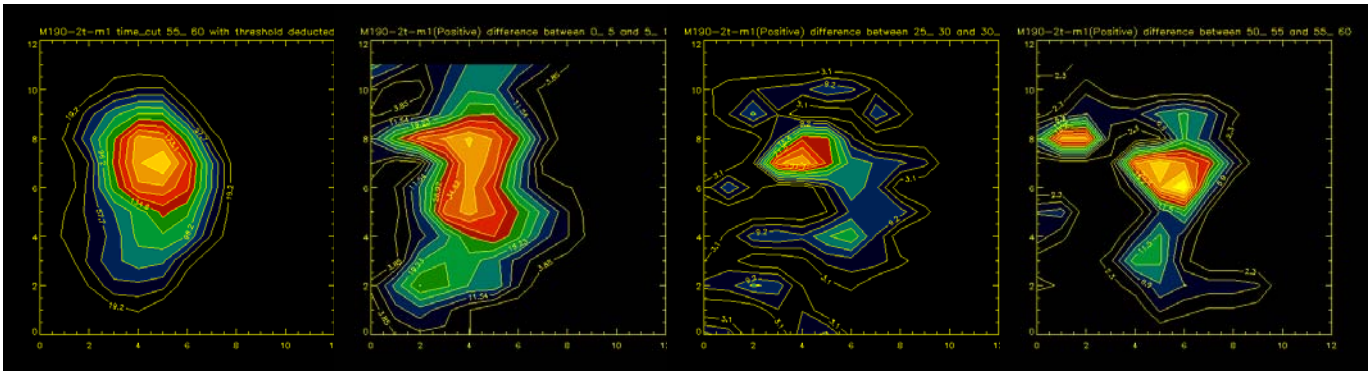

Negative plots indicate that there are only accumulation and no loss of I-125 in the tumor during the first 15 min after injection. However, some regions in the tumor start to lose I-125 at 30 min or earlier after the injection. Comparing the first positive (0-5 min vs. 5-10 min) with the last negative (50-55 min vs. 55-60 min) difference plots (see the figures of mouse 216), we may find that the regions losing I-125 in the right figure match the less active regions in the left figure which are adjacent to the hot regions presenting active NIS expression. This may suggest that the hot regions are actually necrotic tissues in the negative difference plot (50-55 min vs. 55-60 min).

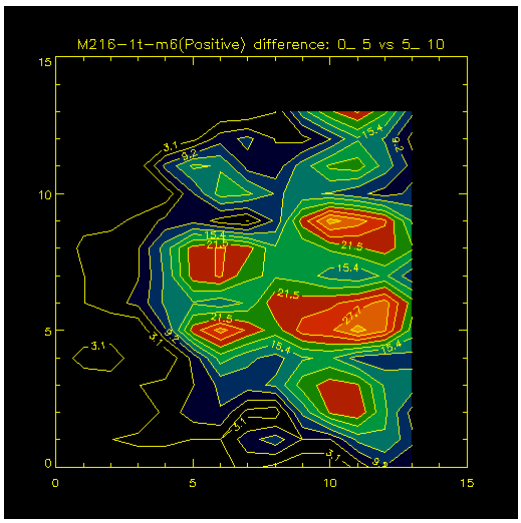

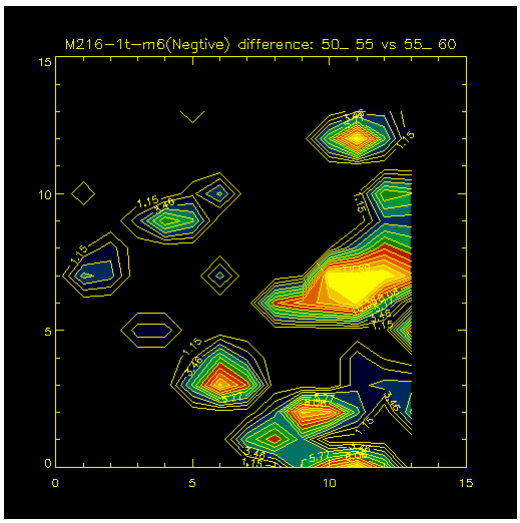

By combining the positive and negative figures, we may find how the isotope is transferred within the tumors with a center-to-edge pattern of I-125 uptake (see the following figures of mouse 212):

1. Initial uptake of I-125 via NIS expression of the active tumor tissues;
2. Then, adjacent tumor tissues become hot with I-125 transferred from the central regions;
3. I-125 is kept on being transferred from the near-central regions to edge regions

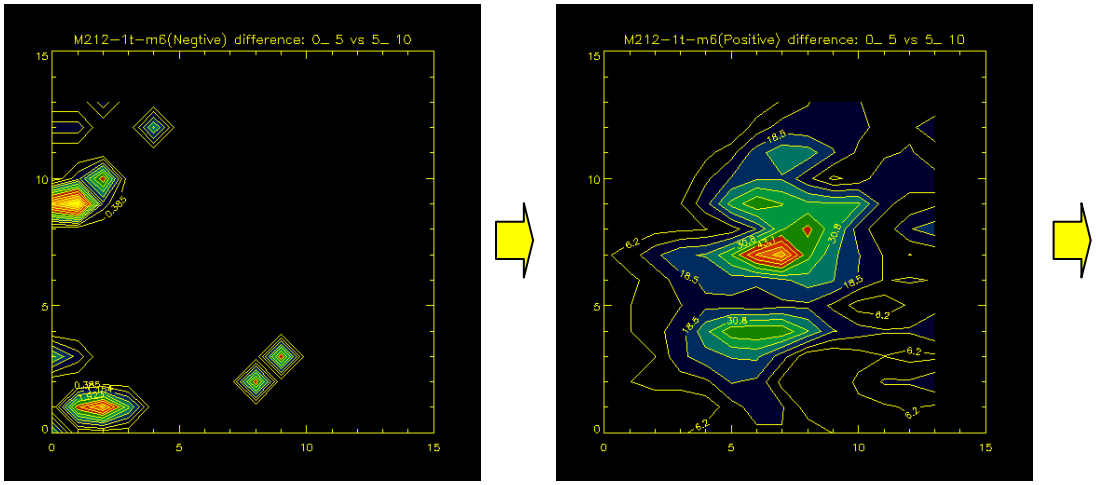
M212−1t−m6(Negtive) difference: 0_ 5 vs 5_ 10
M212−1t−m6(Positive) difference: 0_ 5 vs 5_ 10

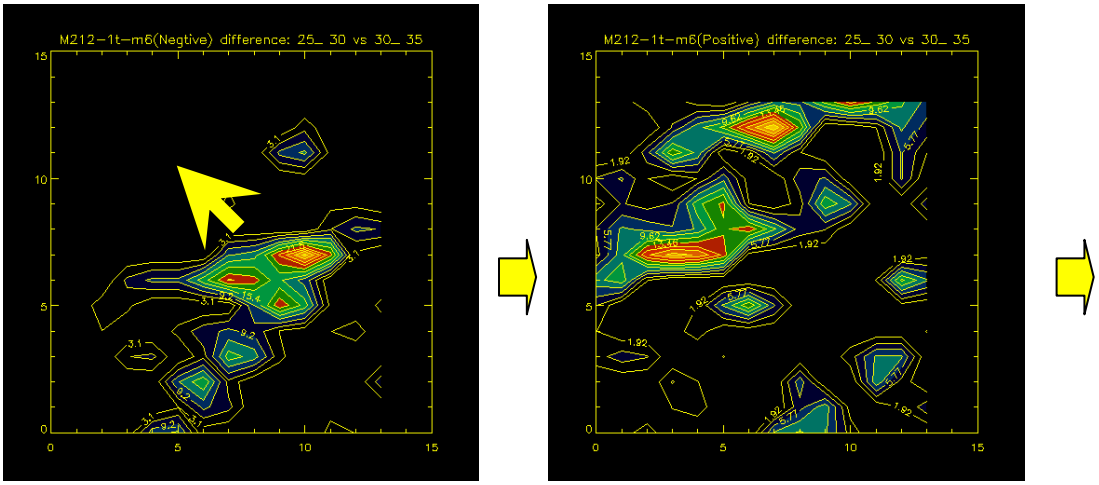
M212−1t−m6(Negtive) difference: 25_ 30 vs 30_ 35
M212−1t−m6(Positive) difference: 25_ 30 vs 30_ 35

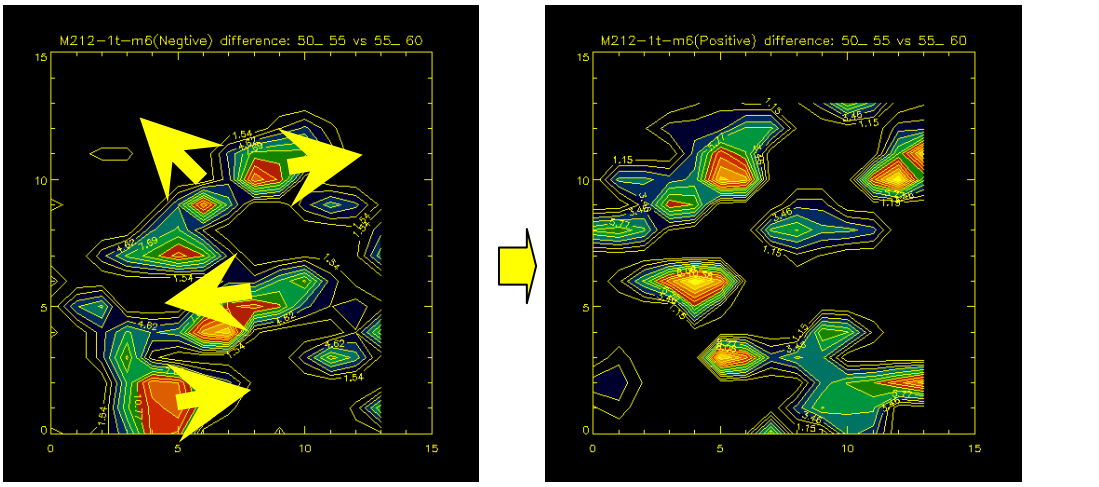
M212−1t−m6(Negtive) difference: 50_ 55 vs 55_ 60
M212−1t−m6(Positive) difference: 50_ 55 vs 55_ 60

9. Correlation between NMGs of C57 Mice and Immunohistochemistry

Two sets of C-57 mice were imaged to verify the correlation between the gamma-ray imaging and immunohistochemistry. Each set includes a lactating mouse, a virgin mouse and a mouse who was lactating but not now (I called it non-lactating mouse). For the first set, we averaged the normalized 3x3 ROIs of three normal mammary glands (NMGs) of each mouse and achieved the following figure.

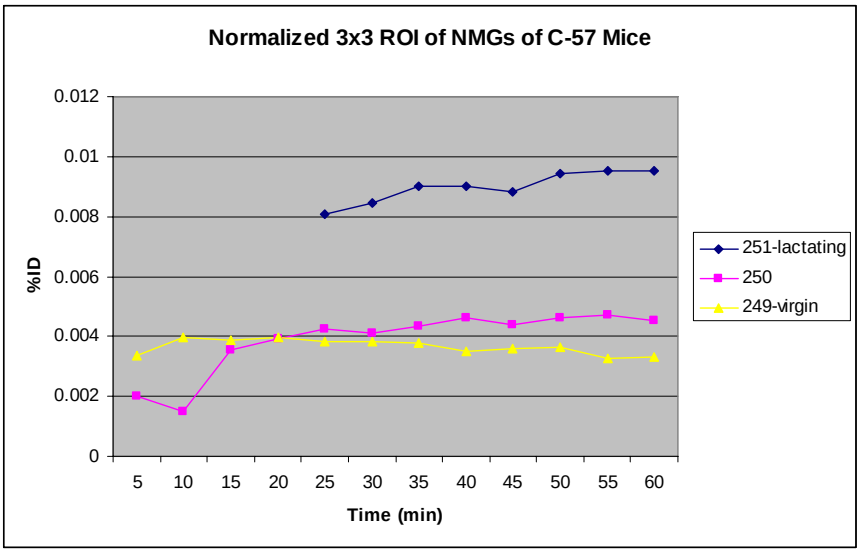

The I-125 level in the NMGs of C-57 mice is in the order of virgin, non-lactating and lactating, which is correlated with immunohistostaining results. Comparing this figure with the following figure showing MMTV mammary glands bearing no palpable tumors, we find that I-125 level in some of these MMTV mammary glands are above the NMGs of the virgin C-57 mouse and even the non-lactating mouse, suggesting NIS expression may be induced by MMTV in the mammary glands without palpable tumors.

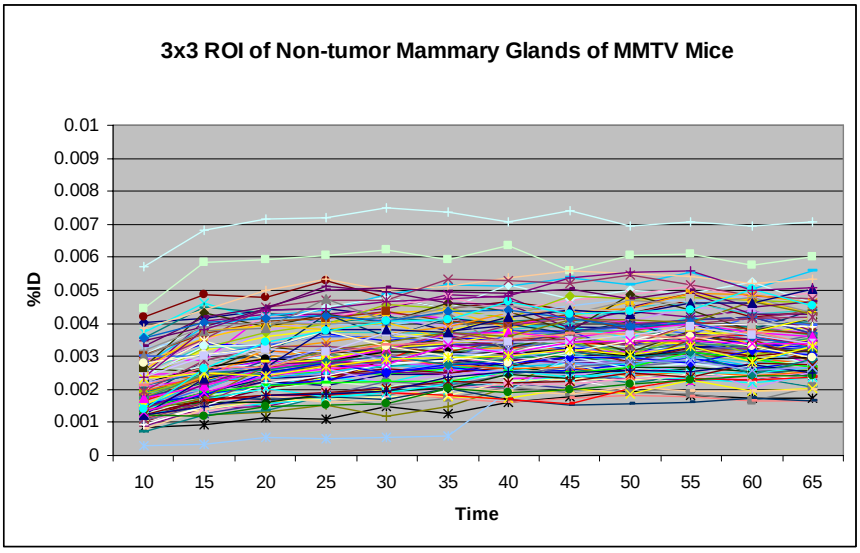

The second set of C-57 mice presents a different trend from the first set (see the following figure). In this trend, the I-125 level in the non-lactating mouse is almost identical with the virgin mouse. Neither virgin or previously lactating mice (254 and 255) had visual immunohistochemical signals of NIS. This result is strictly consistent with their I-125 level at 50-55 min (shown in the following figure).

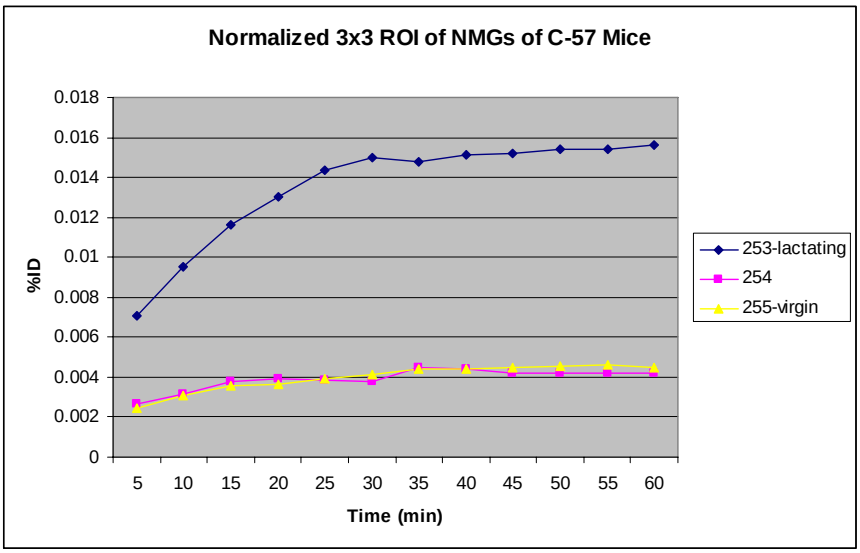

10. Analysis of Tumor Progression (Multiple Imaging)

To achieve as many as possible MMTV cases for summary of tumor propagation, we searched and analyzed the tumors imaged twice or triple times, however, once of which was excluded due to the issue of imaging time or period (< 60 min or a late start time, for example, 30 min after imaging). Finally, we got 11 physical tumors in total (7 mice), in which:

N=2: imaged triple times
N=9: imaged twice

(i) mice with multiple tumors:

mice with	one tumor	two tumors
n	3	4

For mice with two tumors:
N=2: left thoracic + right inguinal
N=2: left and right thoracic

(ii) Tumor location:

tumor location	left thoracic	right thoracic	right inguinal
n	5	4	2

It seems that tumor location is not associated with the following correlations.

mouse #	tumor location	max tumor size	size Increase (%)	normalized mean counts/pixel	change of mean counts/pixel (%)	Pattern	imaging interval (day)	whole tumor
167a-6	right thoracic	13		0.00006		center-to-edge		0.00043
167b-6		23	76.92	0.00014	133.33	center-to-edge	7	0.00230
207-5	right inguinal	22		0.00009		center-to-edge		0.00129
207b-5		41	86.36	0.00011	22.22	center-to-edge	4	0.00425
207-1	left thoracic	39		0.00020		multi-spot		0.00765
207b-1		69	76.92	0.00024	20	multi-spot	4	0.01634
181-1	left thoracic	35		0.00015		multi-spot		0.00448
181c-1		69	97.14	0.00011	-26.67	multi-spot	7	0.00766
181-6	right thoracic	33		0.00010		multi-spot		0.00158
181c-6		94	184.85	0.00018	80	multi-spot	7	0.00950
213-1	left thoracic	31		0.00011		multi-spot		0.00266
213b-1		45	45.16	0.00016	45.45	multi-spot	6	0.00559
213-5	right inguinal	68		0.00045		multi-spot		0.02831
213b-5		65	-4.41	0.00034	-24.44	multi-spot	6	0.02207
178-6	right thoracic	159		0.00044		multi-spot		0.06170
178b (180)-6		407	155.97	0.00024	-45.45	multi-spot	12	0.08039
178-1	left thoracic	13		0.00004		center-to-edge		0.00042
178b (180)-1		23	76.92	0.00006	50	multi-spot	12	0.00083
246-6	right thoracic	60		0.00023		multi-spot		0.01310
246b-6		52	-13.33	0.00021	-8.7	multi-spot	22	0.01046
246c-6		58	11.54	0.00022	4.76	multi-spot	27	0.01097
139-6	right thoracic	24		0.00021		center-to-edge		0.00477
139b-6		52	116.67	0.00025	19.05	center-to-edge	14	0.01284
139c (146)		107	105.77	0.00021	-16	multi-spot	21	0.01918

(iii) Tumor size:

N=9: tumors had increased tumor size
N=2: tumors remained their size.

For the tumors (n=9) imaged twice:

Imaging interval	no increase	slow increase	moderate increase	aggressive
4-7 days	1	1 (<50%)	4 (50%-100%)	1 (>100%)
12 days		1 (<100%)		1 (>150%)

For the tumors (n=2) imaged triple times:
N=1: tumor remained the size
N=1: tumor had a moderate speed (105-120% with intervals of 14-21 days) of propagation across the period.

Summary: A considerable portion (n=4, ~ 50%) of tumors has a moderate speed of propagation while ~20% (n=2) of tumors have no detectable propagation. The speed of tumor propagation has no relationship with the initial size or pattern of the tumor. A large tumor can still be an aggressive tumor.

(iv) Tumor pattern change:

N=9: tumors propagate with no pattern change
N=2: tumors propagate with pattern change from center-to-edge to multi-spot pattern. Both tumors initially have a small size.

Summary: pattern change happens for the initial tumor with a small size. The pattern usually changes from center-to-edge to multi-spot.

(v) Change of mean counts/pixel of the tumor

Mean counts/pixel could be an indicator of the average level of the NIS expression in the tumor.

Summary: the change of mean counts/pixel of a tumor is not clearly correlated with the change of its size except that the tumors (n=2) with no size propagation had either decreased or constant mean counts/pixel.

KEY RESEARCH ACCOMPLISHMENTS

1. We have developed a novel, compact, high resolution gamma-ray detector with a sensitive area measuring 46 mm x 96 mm dedicated for biological study using mouse models; it is capable of detecting iodine-125 metabolism in mammary tumors and its high sensitivity allows us to use much lower doses of radioactive tag.
2. We have extended gamma camera's efficacy to detecting small non-palpable 2-3mm tumors and iodine-125 metabolism in associated mammary glands ofnulliparous tumor-bearing mice.

3. We have developed computer software ROI programs particularly appropriate for the mammary tumor study so that we can accurately determine the important parameters such as tumor size, patterns and trends of iodine uptake.
4. In this collaborative effort it has been confirmed that the immunohistochemical signal for NIS is correlated with the radionuclide intensity in the scintigraphy of MMTV tumors, C57 normal mammary glands (MGs) and MMTV MGs bearing no visual tumors. This strong correlation validates the imaging technique.
5. Corroborated that normal NIS mammary gland expression occurs extensively during lactation in C57 mice suggesting that ^{125}I metabolism in MMTV nulliparous mammary glands may be a hallmark of MMTV tumorigenesis.
6. We have examined nearly 100 mice and have obtained reliable, contolled and usable data from a population of ~ 40 MMTV mice exhibiting over 50 tumors in total for a total of ~60 gamma-ray imaging cases. This has provided data sufficient for statistical interpretation.
7. We have found that MMTV tumors are more likely to be developed in the thoracic regions (over 70% of the tumors) and that MMTV mice exhibit ~ 50 % possibility of developing more than one tumor.
8. We have classified four patterns of iodine uptake in MMTV tumors which we have identified as: edge-to-center, center-to-edge, multi-spot and ring (a special case of multi-spot).
9. The correlation among tumor size, pattern and near-stable iodine uptake (measured 50-55 minutes after the injection) has revealed that small-size tumors (< 75 pixels in area, 1.2 x 1.2 mm^2/pixel) generally exhibit edge-to-center or center-to-edge pattern and have a linear relationship with iodine uptake in them. Moderate-sized and advanced tumors are mostly multi-spot pattern and exhibit two trends in iodine uptake.
10. We have demonstrated that plots of the difference in activity between gamma images taken over two imaging periods have the potential to reveal the pathway of iodine transfer within the tumor.
11. We have demonstrated that gamma-ray imaging is a promising in vivo method to monitor the changes of tumor size, pattern and trends of iodine uptake associated with mammary tumor propagation in the mouse. These may be of significant diagnostic value.

REPORTABLE OUTCOMES

TRAINING

The grant provided significant training for two graduates students in the new interdisciplinary field of in vivo molecular imaging: Jianguo Qian (who will obtain his PhD this fall) and Eric Blue (who will obtain his Masters degree in spring). In addition, several undergraduates were also trained on the project and wish to pursue graduate degrees in this and related fields. These include: Stephen Schworer, Amir Yazdi, and Jonathan Sutton.

Manuscripts: (Graduate student names in bold; undergraduate student names underlined).

Papers In preparation:

Jianguo Qian, **R. Eric Blue**, J. Sutton, A. Yazdi, S. Schworer, Eric L. Bradley, Stan Majewski, Mark F. Smith, Andrew G. Weisenberger, and Robert E. Welsh, Margaret S. Saha. In Vivo Imaging of the Pattern, Size and Iodine Metabolism of Mammary Tumors in MMTV Mice.

Describes the work presented in the body of the report.

Jianguo Qian, **R. Eric Blue**, Eric L. Bradley, Stan Majewski, Margaret S. Saha, Mark F. Smith, Andrew G. Weisenberger, and Robert E. Welsh. "Studies of the mouse thyroid in vivo using multipinhole helical SPECT."

A small-animal imaging system suitable for SPECT imaging and multipinhole standard/helical SPECT has been designed and constructed. Copper-beryllium parallel-hole collimators suitable for imaging the ~35 keV photons from the decay of ^{125}I have been built and installed to achieve better spatial resolution and to reduce imaging time on our dual-detector array. To further address the limitations in the resolution of parallel-hole SPECT and the sensitivity and limited field of view of single-pinhole SPECT, we have incorporated multipinhole circular/helical SPECT in addition to expanding parallel-hole SPECT capabilities. The pinhole SPECT system is based on a 110 mm circular detector equipped with pixellated NaI(Tl) scintillator (1x1x5mm^3/pixel). The helical trajectory is accomplished by two stepping motors controlling the rotation of the detector-support gantry and displacement of the animal bed along the axis of rotation of the gantry. Results obtained in SPECT studies of various phantoms show an enlarged field of view, enhanced resolution and improved sensitivity over our earlier results. In particular, improved reconstructed resolution is obtained with the helical pinhole SPECT. Pinhole collimators with one, three and five 1 mm diameter pinholes have been used in these tests. Spatial resolution of 1.26 mm, 1.43 mm and 1.55 mm have been obtained respectively with those collimators.

Submitted Paper:

Jianguo Qian, Eric L. Bradley, Stan Majewski, Vladimir Popov, Margaret S. Saha, Mark F. Smith, Andrew G. Weisenberger, and Robert E. Welsh. "A small-animal imaging system capable of multipinhole circular/helical SPECT and parallel-hole SPECT." *submitted to Nuclear Instruments and Methods in Physics Research Section A,* June 2007.

We have designed and built a small animal single photon emission computed tomography (SPECT) imaging system equipped with parallel-hole and multipinhole collimators and capable of circular or helical SPECT. Copper-beryllium parallel hole collimators suitable for imaging the ~35 keV photons from the decay of 125I have been built and installed to achieve useful spatial resolution over a range of object-detector distances and to reduce imaging time on our dual-detector array. To address the resolution limitations in the parallel-hole SPECT and the sensitivity and limited field of view of single-pinhole SPECT, we have incorporated multipinhole circular and helical SPECT in addition to expanding the parallel-hole SPECT capabilities. The pinhole SPECT system is based on a 110 mm circular detector equipped with a pixellated NaI(Tl) scintillator array (1×1×5 mm3/pixel).
The helical trajectory is accomplished by two stepping motors controlling the rotation of the detector-support gantry and displacement of the animal bed along the axis of rotation of the gantry. Results obtained in SPECT studies of various phantoms show an enlarged field of view, submillimeter resolution and very good sensitivity using multipinhole circular or helical SPECT. Collimators with one, three and five 1 mm diameter pinholes have been implemented and compared in these tests.

Published Papers:

The work conducted through this DOD grant substantially contributed to this manuscript which is also of interest in the post-911 age and current guidelines for blocking the thyroid with potassium iodide.

Hammond, W., Bradley, E., Welsh, R., **Qian, J.**, Weisenberger, A., Smith, M., Majewski, S., Saha, M.S., "A Gamma Camera Re-evaluation of Potassium Iodide Blocking Efficiency in Mice," vol.92, no.4, pp. 396-406, 2007.

The protection of the thyroid against radioiodine uptake has been an important safety concern for decades. After several studies examined potassium iodide blockade efficacy in the 1960s and 1970s, a standard dosage was prescribed by both the World Health Organization and the US Food and Drug Administration. In this paper, we tested the effectiveness of a scaled version of that standard dosage in comparison to higher doses in mice. A novel gamma camera was employed with a high spatial resolution for precisely quantifying activity within the thyroid and a field of view large enough to image the entire mouse body. Thyroid and whole-body ^{125}I biodistribution was analyzed immediately after exposure and as well as one and seven days later. It was found that one hour after exposure five times the scaled human dose blocked thyroid uptake about 40% more effectively than the 1X scaled dose. Even after 1 day and 7 days, five times the recommended scaled human dose blocked approximately 10% more effectively than the 1X dose. These data suggest the need for continued evaluation of the effectiveness of KI as a blocking agent and the application of novel, non-invasive technologies to this important human health issue.

Eric L. Bradley, Julie Cella, Stan Majewski, Vladimir Popov, **Jianguo Qian**, Margaret S. Saha, Mark F. Smith, Andrew G. Weisenberger, and Robert E. Welsh. "A compact gamma camera for biological imaging." *IEEE Trans. Nucl. Sci.*. vol. 53, no.1, pp. 59-65, 2006

A small-animal imaging system suitable for SPECT imaging and multipinhole standard/helical SPECT has been designed and constructed. Copper-beryllium parallel-hole collimators suitable for imaging the ~35 keV photons from the decay of ^{125}I have been built and installed to achieve better spatial resolution and to reduce imaging time on our dual-detector array. To further address the limitations in the resolution of parallel-hole SPECT and the sensitivity and limited field of view of single-pinhole SPECT, we have incorporated multipinhole circular/helical SPECT in addition to expanding parallel-hole SPECT capabilities. The pinhole SPECT system is based on a 110 mm circular detector equipped with pixellated NaI(Tl) scintillator (1x1x5mm^3/pixel). The helical trajectory is accomplished by two stepping motors controlling the rotation of the detector-support gantry and displacement of the animal bed along the axis of rotation of the gantry. Results obtained in SPECT studies of various phantoms show an enlarged field of view, enhanced resolution and improved sensitivity over our earlier results. In particular, improved reconstructed resolution is obtained with the helical pinhole SPECT. Pinhole collimators with one, three and five 1 mm diameter pinholes have been used in these tests. Spatial resolution of 1.26 mm, 1.43 mm and 1.55 mm have been obtained respectively with those collimators.

Presentations:

***Accepted by IEEE Nuclear Science Symposium and Medical Imaging Conference,* Honolulu, HI, Oct. 28 – Nov. 3, 2007. *In Vivo* Multipinhole Helical SPECT of a Mouse Thyroid**

Jianguo Qian, *Student Member, IEEE*, **R. Eric Blue**, Eric L. Bradley, Stan Majewski, Margaret S. Saha, *Member, IEEE*, Mark F. Smith, *Member, IEEE*, Andrew G. Weisenberger and Robert E. Welsh

Multipinhole single photon emission computed tomography (SPECT) and single-pinhole helical SPECT have been used to advantage in small animal imaging. We have developed a compact multi-function small-animal imaging system which can acquire either multipinhole circular/helical SPECT or parallel-hole SPECT. In anticipation of small animal studies, we have, using phantoms, shown earlier that this system provides an enlarged field of view, submillimeter reconstruction resolution and enhanced sensitivity. In the present work reported here, we demonstrate the utility and proof of concept of this system by imaging a mouse thyroid in vivo with using multipinhole helical SPECT in which the collimator had two pinholes. The thyroid is a particularly useful system for imaging given that the sodium idodide symporter (NIS) mediates uptake of iodine into the thyroid. The mouse was injected with 100-200 µCi ^{125}I and imaged in vivo 24 hours later when about approximately 10-20 µCi were still

remained in the thyroid. The presence of NIS in the thyroid was confirmed with immunocytochemistry. Two-pinhole helical SPECT scans with a magnifying factor of 3 were successfully carried out for 2-4 hours with no overlapping area of the thyroid projections from both pinholes. The mouse was put 2.5 cm from the collimator which results in a total field of view of 20.4 cm^2. The reconstruction results of a 30 gram mouse (C57-derived, MMTV infected female) show the two clearly resolved lobes of the mouse thyroid, suggesting the potential application of multipinhole helical SPECT in studies of thyroid diseases and the potential for better understanding of mouse thyroid physiology.

2006 Academy of Molecular Imaging Annual Conference, March 25-29, 2006
A compact small-animal imaging system incorporating parallel-hole SPECT and multipinhole standard/helical SPECT

Jianguo Qian, Eric L.Bradley, Stan Majewski, Vladimir Popov, Margaret S. Saha, Mark F. Smith, Andrew G. Weisenberger, Robert E. Welsh, and Randolph Wojcik.

We have incorporated multipinhole helical (and ordinary) single photon emission computed tomography (SPECT) in our parallel-hole SPECT imaging system. Previous efforts have demonstrated the utility of parallel-hole SPECT with this system based on two detectors incorporating Hamamatsu R3292 PSPMTs. Recent expansion with a "mouse-sized" detector incorporating a pair of 2"x2" Hamamatsu H8500 modules enhanced the system further. To address limitations in spatial resolution of our parallel-hole detectors and the sensitivity of our detectors with single-pinhole collimators we have tested a combination of multipinhole and helical SPECT with enlarged field of view and enhanced resolution and sensitivity. The multipinhole SPECT system is based on the 110mm circular detector equipped with pixellated (1x1x5mm3/pixel) NaI(Tl) scintillator on a rotating gantry. A helical orbit was effected by adding a rack providing movement of the animal along the axis of rotation of the gantry. The system is capable of organ-specific multipinhole SPECT or whole-body multipinhole helical SPECT. Features are compared among the various modes based on phantom studies.

2006 Users Workshop and Annual Meeting at Jefferson Lab, June 12-14, 2006
A Compact System for Small Animal Nuclear Imaging

Jianguo Qian, Eric L.Bradley, Stan Majewski, Vladimir Popov, Margaret S. Saha, Mark F. Smith, Andrew G. Weisenberger, and Robert E. Welsh

Single photon emission computed tomography (SPECT) is now a well established imaging technique. It has shown great promise in small animal imaging for biological studies. Previously, we have demonstrated the utility of parallel-hole SPECT with a compact system based on two detectors incorporating Hamamatsu R3292 position sensitive photomultiplier tubes (PSPMTs). We have recently enhanced the system with a compact "mouse-sized" detector incorporating a pair of 2"x2" Hamamatsu H8500 PSPMTs. To further address limitations in spatial resolution of the parallel-hole detectors and the sensitivity of detectors with single-pinhole collimators we have expanded the system to include a combination of multipinhole and helical SPECT with an enlarged field of view and enhanced resolution and sensitivity. The multipinhole SPECT system is based on the 110 mm circular detector equipped with pixellated (1x1x5 mm3/pixel) NaI(Tl) scintillator on a rotating gantry. A helical orbit for rotation of the detector about the animal has been accomplished by adding a rack providing movement of the animal along the axis of rotation of the gantry. Features are compared among the various modes of the system based on studies with radioactive phantoms.

2006 Nuclear Science Symposium, Medical Imaging Conference and 15th International Room

Temperature Semiconductor Detector Workshop, October 29 – Nov. 4, 2006
A Multi-Function Compact Small-Animal Imaging System Incorporating Multipinhole Standard and Helical SPECT and Parallel-hole SPECT

Jianguo Qian, *Student Member, IEEE*, Eric L. Bradley, Stan Majewski, Vladimir Popov, Margaret S. Saha, *Member, IEEE*, Mark F. Smith, *Member, IEEE*, Andrew G. Weisenberger and Robert E. Welsh

A small-animal imaging system suitable for SPECT imaging and multipinhole standard/helical SPECT has been designed and constructed. Copper- beryllium parallelhole collimators suitable for imaging the ~35 kev photons from the decay of I-125 have been built and installed to achieve better reconstructed resolution and to reduce imaging time on our dual-detector array. To further address the limitations in the resolution of parallel-hole SPECT and the sensitivity and limited field of view of single-pinhole SPECT, we have incorporated multipinhole standard/helical SPECT in addition to expanding parallel-hole SPECT capabilities. The pinhole SPECT system is based on a 110 mm circular detector equipped with pixellated NaI(Tl) scintillator (1x1x5mm3/pixel). The helical trajectory is accomplished by two stepping motors controlling the rotation of the detector-support gantry and displacement of the animal bed along the axis of rotation of the gantry. Results obtained in SPECT studies of various phantoms show an enlarged field of view, enhanced resolution and improved sensitivity over our earlier results. In particular, improved spatial resolution is obtained with the helical pinhole SPECT. Pinhole collimators with one, three and five 1 mm diameter pinholes have been used in these tests. Spatial resolution of 1.26 mm, 1.43 mm and 1.55 mm have been obtained respectively with those collimators.

Upcoming Regional Meetings:

American Physical Society Regional Meeting (Fall, 2007)
Scintillation Studies of the Mouse Mammary Tumor Virus with ^{125}I

Amir Yazdi[1], **Eric Blue[2],**Eric L. Bradley[2,3], Stan Majewski[4], Shira Mohammed[2], **Jianguo Qian [3],** Margaret S. Saha[2], Stephen Schworer[2], Jonathan Sutton[1]Andrew Weisenberger[4] and Robert E.Welsh[1]
[1] Physics Department; [2] Biology Department and [3] Applied Science Department, The College of William and Mary; [4]Thomas Jefferson Lab Detector and Imaging Group

We have applied the techniques of scintillation imaging to studies of the mouse mammary tumor virus (MMTV). In these studies, the Sodium Iodide Symporter (NIS) transfers the radioactive ^{125}I (in the form NaI) to the mammary glands of lactating mice and in particular to those mammaries with visible tumors. These studies have principally been carried out using pixellated scintillators coupled to position sensitive photomultiplier tubes (PSPMTs). More recently, we have initiated such studies with a monolithic slab of $LaBr_3$ scintillator coupled to an array of PSPMTs. Several techniques of mapping and measuring the development of such tumors have been employed. These will be discussed in detail and preliminary results will be reported.

American Physical Society Regional Meeting (Fall, 2007)
Development and Testing of a Novel Lanthanum Bromide Scintillation Detector for SPECT Imaging

Jonathan Sutton[1], Eric L. Bradley[2,3], Stan Majewski[4], John McKisson [4], Vladimir Popov[4], James Proffitt[4], **Jianguo Qian [3],** Margaret S. Saha[2], Andrew Weisenberger[4] ,Robert E.Welsh[1] and Amir Yazdi[1]
[1] Physics Department; [2] Biology Department and [3] Applied Science Department, The College of William and Mary; [4]Thomas Jefferson Lab Detector and Imaging Group

A single piece of $LaBr_3$ has been coupled (by Bicron-St Gobain Inc.) to four special position sensitive phototubes (PSPMTs; Hamamatsu, Inc.) to create a novel detector for biological imaging with high sensitivity, very good energy resolution and high spatial resolution. The $LaBr_3$ scintillator is coupled

to four Hamamatsu H9500 PSPMTs and the resulting detector can be used with parallel or pinhole collimation. To reduce the number of active channels, novel additive resistive readout circuitry has been implemented. In addition, we have applied special techniques to the achievement of spatial uniformity across the 100 mm^2 face of the detector. This technique is of special importance at the interfaces of the four square PSPMTs where the continuous scintillator must act to spread the light between the two photosensitive devices due to the reduced sensitivity in these regions. To map the detected gamma rays to their actual grid locations on the detector, a special drilled mask has been used to generate a uniform array of spots which can then be used to generate a corrective matrix. These techniques and results obtained will be described and discussed.

CONCLUSIONS

In vivo imaging has emerged as the next cutting edge tool for research. This technology equips one to analyze previously obscure biological processes in a real time fashion. The gamma camera is a novel *in vivo* imaging system presented here that examines the capacity for ^{125}I metabolism in mouse MMTV tumors to which this metabolic pathway is subject to the NIS. Molecular biology data has validated the gamma camera's efficacy by localizing the NIS in MMTV tumors that highly reflect ^{125}I saturation in gamma images. Since tumor size (volume) is probably the most important parameter in the correlations we have found, more precisely determined tumor size will substantially authenticate those correlations. As we have proved in detector development, SPECT imaging is able to reconstruct the three-dimensional distribution of radioiodine in MMTV tumors suggesting the potential of determining not only the tumor volume but also the 3-D patterns of radioiodine uptake in the tumor. Planar gamma-ray imaging has been demonstrated an effective way in our study to investigate the dynamic tumor response to radioiodine especially in the first 10-20 minutes after the injection and to determine the tumor size and pattern in an approximate manner due to the limitation of 2-D space. By combining the tomography and planar scintigraphy, we may have the ability to find the correlations and to determine both the dynamic and near-stable behaviors of tumors precisely.

v Our molecular imaging results also suggest the possible correlations among tumor pattern, size and pathology such as solid or soft tumor and the potential correlations associated with mammary tumor propagation in the mouse, both of which require further studies. Our imaging system itself has detected four radioiodide metabolic patterns correlating with the size of the tumor. Small tumors tend to be morphologically solid with a strong central uptake pattern. Moderate tumors have both variable morphologies as well as ^{125}I uptake patterns. At this stage tumors are either destined to retain their morphology or begin necroses; thus, patterning varies from central/edge saturation to speckled (multi-spot) ^{125}I incorporation. Large tumors generally have blood pools attributed to necrosis and are identified with both speckled (multi-spot) and ring uptake patterns. Tumor propagation patterns have indicated that most tumors preserve the initial uptake pattern as they enlarge, but small tumors did show an inclination to change uptake patterns as they grew.

The correlations among tumor pattern, size and iodine uptake in the tumor may have potential pathological and physiological meanings leading to better understanding and eventually better treatment of tumors. We have also demonstrated that radionuclide scintigraphy is not only an imaging technique for effectively detecting the presence and location of an early-stage tumor but also a promising method for in vivo study of tumor development and propagation. As we know, there is tremendous incentive for detecting cancer at its earliest stage because treatment at that stage is often curative. Using the conventionally available radiotracer $Na^{125}I$, we have been able to detect the non-palpable tumors as small as 3 mm. Moreover, we have noticed in many MMTV cases that mammary glands baring no visual tumors have clear uptake of I-125 in contrast to imaging studies of nulliparous C57 cases, suggesting potential tumor development. Therefore, sodium iodide may be a promising radiotracer for detecting non-palpable tumors at the earliest stage. On the other hand, *in vivo* gamma-ray imaging makes it possible to observe a tumor at different stages with respect to the size, pattern

and iodine uptake. The *in vivo* study of tumor propagation has significant therapeutical meaning such as monitoring tumor response to pharmaceuticals.

This research is geared toward an applicable way to image and detect mammary tumors in a safe and expeditious manner. The ultimate goal of our research is to provide a reliable way to predict where a tumor will manifest and the morphology of the tumor based on metabolic patterning. The gamma camera technology is essential for advancing *in vivo* research that would limit the amount of invasive techniques currently employed. Invasive procedures while informative only give partial information representing a snap shot of the organism at a set time. To rectify this dilemma *in* vivo imaging can functionally assess biological processes over a period of time in a live animal. In the future we hope to include pinhole imaging to offer three-dimensional information about MMTV tumors and procure a more in depth analysis of ^{125}I metabolism. Additionally, we would like to attain gene libraries specific to mouse breast cancer/estrogen receptor signaling via microarrays to distinguish which genes relating to breast cancer are expressed in MMTV tumors. We are also beginning to analyze real-time PCR technology to quantitatively differentiate between NIS expression between mammary tumors and associated mammary glands of tumor baring mice. Likewise, we are currently cell culturing MMTV tumor cells for both immunocytochemistry and gamma imaging. We want the cultured tumor cells to inject into the mammary glands of mice with no tumors to distinguish if the cells themselves can propagate the formation of a tumor. Additional research will combine the use of cell culture techniques, molecular biology and imaging to focus on tumor stem cells—a promising area for diagnostics and therapy—particularly when combined with novel imaging technology.

Overall, the research conducted during the past year has indicated that the use of I-125 labeled NaI has significant potential for the early diagnosis and the potential prognosis for mammary tumors. Uptake of the radiolabel is significantly higher in all tumors than in background tissue, making the tumors visible non-invasively. Moreover, as seen from the images present above, the label is able to display the different types and physiology of the tumors and to reveal their considerable heterogeneity – all non-invasively. This research is of obviously importance and significance to the broader community and to the general public because of the need to develop more non-invasive methods of detecting tumors and providing reasonable and accurate prognoses. Moreover, these non-invasive techniques must employ minimal side effects. The very sensitive detector system we have developed for mammy imaging in small mammals allows for a very low level of radioactive material, in the range of 10 to 100 fold lower than in other imaging systems. However, additional work must be performed. First it will be important to test the utility of I-125 labeled NaI in other model systems as well to determine if our findings can be extended to a variety of tumors. Secondly, future work will include a careful molecular analysis of the tumors and correlation of these data with the imaging and physiological data. Thirdly, hypotheses generated from our data (e.g. the possible suppression of NaI uptake in mammary glands in mice bearing tumors) will be tested to determine potentially novel non-invasive imaging strategies that could be of use with novel therapies (Dadachova et al, 2005; Dwyer et al., 2005; Kogai et al., 2004; Wapnir et al., 2004).

REFERENCES

Cho JY. (2002). A transporter gene (sodium iodide symporter) for dual purposes in gene therapy: imaiging and therapy. Curr Gene Ther. 2(4):393-402.

Chung JK. (2003). Sodium iodide symporter: its role in nuclear medicine. J Nucl Med. 43(9):1188-200.

Dadachova E, Carrasco N. (2004). The Na/I symporter (NIS): imaging and therapeutic applications. Semin Nucl Med. 34(1):23-31

Dadachova E, Nguyen A, Lin EY, Gnatovskiy L, Lu P, Pollard JW. (2005). Treatment with rhenium-188-perrhenate and iodine-131 of NIS-expressing mammary cancer in a mouse model remarkably inhibited tumor growth. Nucl Med Biol. 2005 Oct;32(7):695-700

Dadachova E, Zuckier LS. (2003). Overlooked contributions on sodium iodide symporter. J Nucl Med. 44(10):1707.

Dwyer RM, Bergert ER, O'Connor MK, Gendler SJ, Morris JC. (2005). In vivo radioiodide imaging and treatment of breast cancer xenografts after MUC1-driven expression of the sodium iodide symporter. Clin Cancer Res.11(4):1483-9.

Kogai T, Kanamoto Y, Che LH, Taki K, Moatamed F, Schultz JJ, Brent GA. (2004). Systemic retinoic acid treatment induces sodium/iodide symporter expression and radioiodide uptake in mouse breast cancer models. Cancer Res. 64(1):415-22.

Moon DH, Lee SJ, Park KY, Park KK, Ahn SH, Pai MS, Chang H, Lee HK, Ahn IM. (2001). Correlation between 99mTc-pertechnetate uptakes and expressions of human sodium iodide symporter gene in breast tumor tissues. Nucl Med Biol. 28(7):829-34.

Wapnir IL, Goris M, Yudd A, Dohan O, Adelman D, Nowels K, Carrasco N. (2004). The Na+/I- symporter mediates iodide uptake in breast cancer metastases and can be selectively down-regulated in the thyroid Clin Cancer Res. 10(13):4294-302.